

Effect of Feshbach resonance on dynamics of matter waves in optical lattices

V.A. Brazhnyi^{1*} and V.V. Konotop^{1,2†}

¹*Centro de Física Teórica e Computacional, Universidade de Lisboa,
Complexo Interdisciplinar, Av. Prof. Gama Pinto 2, Lisboa 1649-003, Portugal*

²*Departamento de Física, Faculdade de Ciências, Universidade de Lisboa,
Campo Grande, Ed. C8, Piso 6, Lisboa 1749-016, Portugal.*

Mean-field dynamics of a Bose-Einstein condensate (BEC) loaded in an optical lattice (OL), confined by a parabolic potentials, and subjected to change of a scattering length by means of the Feshbach resonance (FR), is considered. The system is described by the Gross-Pitaevskii (GP) equation with varying nonlinearity, which in a number of cases can be reduced a one-dimensional perturbed nonlinear Schrödinger (NLS) equation. A particular form of the last one depends on relations among BEC parameters. We describe periodic solutions of the NLS equation and their adiabatic dynamics due to varying nonlinearity; carry out numerical study of the dynamics of the NLS equation with periodic and parabolic trap potentials. We pay special attention to processes of generation of trains of bright and dark matter solitons from initially periodic waves.

PACS numbers: 03.75.Lm, 03.75.Kk, 05.45.Yv

I. INTRODUCTION

During the last decade Bose-Einstein condensates (BECs) of atomic vapors attracted a great deal of attention of the physical community (see e.g. review papers [1, 2]). Creation and management of spatially localized and periodic matter waves have become the issues of particular importance, optical lattices (OLs) being viewed as one of the most promising tools for that [3, 4] (see also [2] and reference therein). On the other hand, it has been predicted theoretical [5] works and confirmed in experiments [4, 6] that another tool – the Feshbach resonance (FR) – can be effectively employed for manipulating BECs. It also has been suggested that by changing external magnetic field near the resonant point (i.e. by controlling the magnitude and even sign of the s-wave scattering length) one can generate trains of solitons starting with periodic matter wave [7], create stable localized structures such as breathers, 2-soliton states or nearly static states with nested dark solitons [8], compress solitary waves up to high densities [9], and generate shock waves [10] in BECs. Subsequently, a natural question about combined effect of FR and periodic external potential, can be posed. This issue has already been addressed in Ref.[11], where the effect of variations of the scattering length on the dynamics of a soliton of a discrete nonlinear Schrödinger (NLS) equation which simulates an array of BECs in a deep OL within the framework of the tight-binding approximation [12]. However, as it was shown in [13] the latter approximation does not reproduce all features of dynamics of real continuous system, what requires extending consideration beyond the tight-binding limit.

The aim of the present paper is to consider effect of

FR on dynamics of a BEC in reduced one-dimensional (1D) and truly 3D mean-field models. More specifically, we extend the ideas reported in Ref. [7] to the case of BECs embedded in OLs and consider the effect of FR on dynamics of nonlinear Bloch states resulting in creation of trains of bright and dark solitons.

The problem allows rather complete analytical description in a 1D case. That is why we start by listing in Sec. II the main 1D reductions of the 3D Gross-Pitaevskii (GP) equation for different choices of the relation among characteristic scales of the problem. Next, in Sec. III we recall some relevant facts of the theory of the NLS equation which will lead us to simple picture of the effect of varying nonlinearity on one-dimensional periodic solutions. We develop adiabatic approximation, providing some details to the earlier results of Ref. [7] which have applications to the cases when the lattice constant is of order of the transverse size of the cigar-shaped condensate. In Sec. IV adiabatic approximation is applied to describe the dynamics of a periodic matter wave loaded in a periodic potential and affected by FR. Next, in Sec. V we provide numerical study of the 1D dynamics of solutions describing BEC in an OL of relatively small extent. Sec. VI is devoted to direct numerical simulations of the 3D GP equation. The results are summarized in Conclusion. For the sake of convenience some relevant results of the Inverse Scattering technique (IST) and elliptic integrals are given in Appendixes.

*Electronic address: brazhnyi@cii.fc.ul.pt

†Electronic address: konotop@cii.fc.ul.pt

II. EFFECTIVE 1D EQUATIONS

A. Mean-field approximation and parameters of the problem

As is customary we start with the GP equation for the macroscopic wave function $\Psi(\mathbf{r}, t)$:

$$i\hbar\partial_t\Psi = -\frac{\hbar^2}{2m}\Delta\Psi + V(\mathbf{r})\Psi + g_0|\Psi|^2\Psi \quad (1)$$

where we use the standard notations: $g_0 = 4\pi\hbar^2 a_s/m$, a_s is the s -wave scattering length, and m is the atomic mass. The external potential, $V(\mathbf{r})$, is given by $V(\mathbf{r}) = V_{trap}(\mathbf{r}) + V_{latt}(x)$ where $V_{trap}(\mathbf{r}) = \frac{m}{2}(\omega_\perp^2 r_\perp^2 + \omega_0^2 x^2)$ is the magnetic trap potential, $\mathbf{r}_\perp = (y, z)$, ω_\perp and ω_0 are the transverse and axial harmonic oscillator frequencies, and $V_{latt}(x) = V_{latt}(x + \Lambda)$ is a lattice potential with the lattice constant Λ proportional to the laser wavelength. The wave function is normalized to the total number of atoms, \mathcal{N} : $\int |\Psi|^2 d\mathbf{r} = \mathcal{N}$.

We consider a cigar-shaped trap when the transverse linear oscillator length, $a_\perp = \sqrt{\hbar/m\omega_\perp}$, is much smaller than the longitudinal one, $a_0 = \sqrt{\hbar/m\omega_0}$: $a_\perp \ll a_0$. Then the condensate becomes a quasi-1D system. In literature there exist several approximations reducing the original GP equation to different effective 1D models. The method allowing one to do that in a controlled manner, i.e. appreciating the neglected terms with a well defined small parameter of the problem, is the multiple scale expansion. The resulting 1D models depend on the relations among the parameters of the problem. The four relevant cases are summarized in the Table I. To discuss them we introduce the healing length $\xi = (8\pi n|a_s|)^{-1/2}$, where $n \approx \mathcal{N}/a_\perp^2 a_0$ is a mean particle density, and thus collect four characteristic spatial scales: $\{a_0, a_\perp, \Lambda, \xi\}$. For the next step we introduce a small parameter of the problem, ϵ , defining it through a ratio between the energy of two-body interactions, $\sim \hbar^2 a_s n/m$, and kinetic energy of the transversal excitations, $\sim \hbar^2/m a_\perp^2$:

$$\epsilon^2 = \frac{a_\perp^2}{\xi^2} \sim \frac{\mathcal{N} a_s}{a_0}. \quad (2)$$

Then, considering possible relations among the characteristic scales with respect to the small parameter ϵ one can single out four different cases which can be treated by means of the multiple-scale expansion. Some of these cases have already considered in details in [14, 15], that is why below we only outline derivation of the respective 1D models.

B. Long trap and rapidly varying OL

Let us start with the Case 1 from Table I, for which the lattice period is of the order of the transverse oscillator length and much less than the healing length:

$a_\perp \sim \Lambda \sim \epsilon\xi \lesssim \epsilon^2 a_0$ (see also [14]). In this case the condensate is rather long and the periodicity modifies the spectrum of the underlying linear system. We introduce dimensionless independent variables $\tilde{t} = \omega_\perp t/2$, $\tilde{x} = x/a_\perp$, $\tilde{\mathbf{r}}_\perp = \mathbf{r}_\perp/a_\perp$, and a renormalized wave function $\tilde{\Psi} = a_\perp |a_s|^{1/2} \Psi$ allowing us to rewrite Eq. (1) in the dimensionless form

$$i\partial_{\tilde{t}}\tilde{\Psi} = \left(\mathcal{L}_\perp + \mathcal{L}_0 + 8\pi\sigma|\tilde{\Psi}|^2\right)\tilde{\Psi}, \quad (3)$$

$$\mathcal{L}_\perp = -\Delta_\perp + \tilde{r}_\perp^2, \quad \mathcal{L}_0 = -\partial_{\tilde{x}}^2 + \nu^2 \tilde{x}^2 + \kappa^2 U(\kappa\tilde{x}).$$

Hereafter $\sigma = \text{sign}(a_s)$, $\nu = \omega_0/\omega_\perp$ is the aspect ratio of the trap, $U(\kappa\tilde{x}) \equiv V_{latt}(x)/E_R$ is a dimensionless periodic potential which is varying on a unit scale, $E_R = \hbar^2 \pi^2 / (2\Lambda^2 m)$ is the recoil energy, and $\kappa^2 = \frac{E_R}{\hbar\omega_\perp} \sim \frac{a_\perp^2}{\Lambda^2}$.

Next we consider linear eigenvalue problems

$$\mathcal{L}_0 \phi_{nq}(\tilde{x}) = \mathcal{E}_{nq} \phi_{nq}(\tilde{x}), \quad (4)$$

$$\mathcal{L}_\perp \xi_{l_1 l_2}(\tilde{\mathbf{r}}_\perp) = \mathcal{E}_{l_1 l_2} \xi_{l_1 l_2}(\tilde{\mathbf{r}}_\perp), \quad (5)$$

Here the indexes n and q stand for the number of a band and wave vector inside the first Brillouin zone (BZ), when it is relevant (cases 1 and 2 in Table I) and the index q must be dropped when the background state is not related to any band structure (cases 2 and 3 in Table I). Indexes $l_{1,2}$ stand for two transverse quantum numbers. The operator \mathcal{L}_0 has a discrete spectrum, which however approximates the band spectrum of the first eigenvalue problem (4) in the limit $\nu \lesssim \epsilon$. In this case the use of the ‘‘band’’ terminology is justified and $\phi_{nq}(x)$ can be approximated by a Bloch function of the respective periodic potential. Below we will restrict the consideration to the Bloch states bordering the edge of the first BZ where $q = q_0 = \pi/\Lambda$, and respectively will use the abbreviated notations $\phi_n(x) \equiv \phi_{nq_0}(x)$ and $\mathcal{E}_n \equiv \mathcal{E}_{nq_0}$. We also will be interested only in the evolution of the background state ($l_1 = l_2 = 0$) of the transverse component: $\xi_{00}(\tilde{\mathbf{r}}_\perp) = \exp(-\tilde{r}_\perp^2/2)/\sqrt{\pi}$, and $\mathcal{E}_{00} = 2$. All eigenfunctions are considered to be normalized to one.

Now we look for a solution of Eq.(3) in a form $\tilde{\Psi} = \epsilon\psi_1 + \epsilon^2\psi_2 + \dots$, where ψ_j ($j = 1, 2, \dots$) are functions of $\tilde{\mathbf{r}}_\perp$ and of scaled independent variables $t_\alpha = \epsilon^\alpha \tilde{t}$ and $x_\alpha = \epsilon^\alpha \tilde{x}$. Then the leading order of the solution can be searched in the form of the weakly modulated ground state

$$\psi_1 = \frac{1}{\sqrt{\pi}} \mathcal{A}_n(x_1, t_2) e^{-i(\mathcal{E}_n+2)t_0} e^{-\tilde{r}_\perp^2/2} \phi_n(x_0), \quad (6)$$

where $\mathcal{A}(x_1, t_2)$ (as well as $\mathcal{B}_n(x_1, t_2)$ below) is a slowly varying envelope amplitude, and by convention we indicate only the most rapid variables (i.e. $\mathcal{A}(x_1, t_2)$ means that \mathcal{A} depends on all $\{x_1, x_2, \dots\}$ and $\{t_2, t_3, \dots\}$).

After substituting expansion of $\tilde{\Psi}$ into (3) one collects the terms at each order of ϵ (for the set of so obtained equations see e.g. [14]). The first order (with respect to ϵ) equation is satisfied by ground state solution (6). A solution of the second order equation reads

$$\psi_2 = \frac{1}{\sqrt{\pi}} e^{-\tilde{r}_\perp^2/2} e^{-i(\mathcal{E}_n+2)t_0} \sum_{n' \neq n} \mathcal{B}_{n'n}(x_1, t_1) \phi_{n'}(x_0) \quad (7)$$

TABLE I: Scaling, backgrounds and effective 1D equations describing matter waves in OLs. All variables in evolution equations are dimensionless (see the text).

Case	Scaling	Background $\phi_n(x_0)$	1D NLS equation
1	$a_\perp \sim \Lambda \sim \epsilon\xi \lesssim \epsilon^2 a_0$	\approx Bloch function	$i\psi_t = -\frac{1}{2M}\psi_{xx} + 2\sigma \psi ^2\psi$
2	$a_\perp \sim \Lambda \sim \epsilon\xi \sim \epsilon a_0$	$=$ Bloch function	$i\psi_t = -\frac{1}{2M}\psi_{xx} + 2\sigma \psi ^2\psi + \nu^2 x^2 \psi$
3	$a_\perp \sim \epsilon\Lambda \sim \epsilon\xi \lesssim \epsilon^2 a_0$	$= \pi^{-1/4} e^{-\nu x_0^2/2}$	$i\psi_t = -\psi_{xx} + 2\sigma \psi ^2\psi + U(x)\psi$
4	$a_\perp \sim \epsilon\Lambda \sim \epsilon\xi \sim \epsilon a_0$	$\equiv 1$	$i\psi_t = -\psi_{xx} + 2\sigma \psi ^2\psi + U(x)\psi + \nu^2 x^2 \psi$

where

$$\mathcal{B}_{n_1 n} = \frac{\Gamma_{n_1 n} \partial_{x_1} \mathcal{A}_n}{\mathcal{E}_{n_1} - \mathcal{E}_n} \quad \text{and} \quad \Gamma_{n_1 n} = - \int_0^\Lambda \bar{\phi}_{n_1} \frac{d\phi_n}{dx_0} dx_0.$$

Also it follows from the second order equation that $\partial_{t_1} \mathcal{A} = 0$, i.e. $\mathcal{A} \equiv \mathcal{A}(x_1, t_2)$. Finally, eliminating secular terms from the third order equation we obtain

$$i\partial_{t_2} \mathcal{A}_n + (2M_n)^{-1} \partial_{x_1}^2 \mathcal{A}_n - \chi_n \sigma |\mathcal{A}_n|^2 \mathcal{A}_n = 0, \quad (8)$$

where $\chi_n = 2 \int_0^\Lambda |\phi_n(x_0)|^4 dx_0$ is the effective nonlinearity and

$$\frac{1}{M_n} = 2 + 2 \sum_{n_1 \neq n} \frac{|\Gamma_{n n_1}|^2}{\mathcal{E}_{n_1} - \mathcal{E}_n}$$

is the inverse effective mass.

For simplicity of final notations we make substitutions $\mathcal{A}_n \rightarrow \sqrt{2/\chi_n} \psi$, $t_2 \rightarrow t$, $x_1 \rightarrow x$, and $M_n \rightarrow M$ one obtains from Eq. (8) a dimensionless NLS equation

$$i\partial_t \psi = -\frac{1}{2M} \partial_x^2 \psi + 2\sigma |\psi|^2 \psi \quad (9)$$

(notice that although we use x and t in the last formula their sense is different from the original physical variables). We also emphasize, that the final Eq.(9) does not contain explicitly the parabolic potential and the OL since they both are taken into account by the ground state solution and thus by the coefficients of the obtained equation.

Finally we have to clarify the meaning of the coefficient M_n^{-1} . This can be done, by means of the so-called **kp**-method, known in the solid state physics. Namely, it turns out that in the limit $a_0/\Lambda \rightarrow \infty$ one has $M_n^{-1} = d^2 \mathcal{E}_{nq}/dq^2$ [14].

C. Short trap and rapidly varying optical lattice

Consider now the Case 2 from Table I, where $a_\perp \sim \Lambda \sim \epsilon\xi \sim \epsilon a_0$, i.e. when the condensate size in the axial direction is not large enough and ‘‘boundary’’ effects cannot be neglected. Like in the previous case, the periodicity is of the order of the radial size of the cloud and much less than the healing length, and thus modifies the spectrum of the liner system introducing the effective mass (or group velocity dispersion, using wave terminology).

Mathematically the above assumptions are expressed by the fact that $a_\perp/a_0 \sim \epsilon$ and thus $\nu^2 x^2 = \epsilon^2 \tilde{\nu}^2 x_1^2$, where $\nu = \epsilon^2 \tilde{\nu}$ and $\tilde{\nu}$ is of unity order. That is why one has to redefine the problem (3) as follows

$$i\partial_t \tilde{\Psi} = \left(\mathcal{L}_\perp + \mathcal{L}_0 + \epsilon^2 \tilde{\nu}^2 (\epsilon \tilde{x})^2 + 8\pi\sigma |\tilde{\Psi}|^2 \right) \tilde{\Psi}, \quad (10)$$

$$\mathcal{L}_\perp = -\Delta_\perp + \tilde{r}_\perp^2, \quad \mathcal{L}_0 = -\partial_{\tilde{x}}^2 + \kappa^2 U(\kappa \tilde{x}).$$

Next one can follow the steps described in the preceding subsection, but now with a different operator \mathcal{L}_0 . This naturally leads to a new background, which is now a solution of the Hill equation (4) and thus is nothing but an exact Bloch function (recall that in the previous case the background was only approximated by the Bloch function). Respectively, a new term describing the parabolic potential appears in the resulting 1D equation:

$$i\partial_t \psi = -\frac{1}{2M} \partial_x^2 \psi + \nu^2 x^2 \psi + 2\sigma |\psi|^2 \psi \quad (11)$$

where for the sake of simplicity $\tilde{\nu}$ is substituted by ν and as before (ψ, t, x) stand for $(\sqrt{\chi_n/2} \mathcal{A}_n, t_2, x_1)$.

D. Long trap and smooth optical lattice

Let us turn to the next case from the Table I, where $a_\perp \sim \epsilon\Lambda \sim \epsilon\xi \lesssim \epsilon^2 a_0$. The peculiarity now, is that the periodic potential has the same (or even larger) scale as the healing length (notice that in this case the parabolic potential is wide enough). Thus now $\kappa = \epsilon \tilde{\kappa}$, where κ is defined in (3) and $\tilde{\kappa}$ is of order one. Then $\kappa^2 U(\kappa \tilde{x}) \equiv \epsilon^2 \tilde{U}(x_1)$ where $\tilde{U}(x_1) \equiv \tilde{\kappa}^2 U(\tilde{\kappa} x_1)$. The system (3), is now rewritten in the form

$$i\partial_t \tilde{\Psi} = \left(\mathcal{L}_\perp + \mathcal{L}_0 + \epsilon^2 \tilde{U}(\epsilon \tilde{x}) + 8\pi\sigma |\tilde{\Psi}|^2 \right) \tilde{\Psi}, \quad (12)$$

$$\mathcal{L}_\perp = -\Delta_\perp + \tilde{r}_\perp^2, \quad \mathcal{L}_0 = -\partial_{\tilde{x}}^2 + \nu^2 \tilde{x}^2.$$

The eigenvalue problem for \mathcal{L}_0 is solved explicitly giving the Gaussian background $\phi_0(x_0) = \pi^{-1/4} \exp(-\nu x_0^2/2)$, and the final (i.e. already in dimensionless units) 1D equation of motion reads

$$i\partial_t \psi = -\partial_x^2 \psi + U(x)\psi + 2\sigma |\psi|^2 \psi. \quad (13)$$

Here $\tilde{U}(x)$ is substituted by $U(x)$. Thus as one could expect the periodic potential appears in the evolution equation in an explicit form.

E. Short magnetic trap and smooth optical lattice

Finally, if one considers not too long condensate and in a lattice having a period of order of the healing length, i.e. the situation described in Table I as Case 4: $a_{\perp} \sim \epsilon\Lambda \sim \epsilon\xi \sim \epsilon a_0$, the both lattice and trap potentials will appear in the final equation of motion. The corresponding problem is reformulated now as follows

$$i\partial_t \tilde{\Psi} = \left(\mathcal{L}_{\perp} + \mathcal{L}_0 + \epsilon^4 \tilde{\nu}^2 \tilde{x}^2 + \epsilon^2 \tilde{U}(\epsilon \tilde{x}) + 8\pi\sigma |\tilde{\Psi}|^2 \right) \tilde{\Psi} \quad (14)$$

$$\mathcal{L}_{\perp} = -\Delta_{\perp} + \tilde{r}_{\perp}^2, \quad \mathcal{L}_0 = -\partial_{\tilde{x}}^2.$$

The ground state as a solution of the linear eigenvalue problems (4) becomes $\phi_n(x_0) \equiv 1$.

Skipping the intermediate calculations similar to ones presented in the Case 1 we write down the final form of the effective 1D equation

$$i\partial_t \psi = -\partial_x^2 \psi + \nu^2 x^2 \psi + U(x)\psi + 2\sigma |\psi|^2 \psi \quad (15)$$

where as before the tildes are suppressed.

III. NLS EQUATION WITH TIME DEPENDENT NONLINEARITY. ADIABATIC THEORY

It turns out that two of the above cases, namely Cases 1 and 3 (Table I), allow rather complete description within the framework of the perturbation theory, while the Cases 2 and 4 where the parabolic potential is explicitly included in the evolution equation for the slowly varying amplitude, have to be studied by means of numerical simulations. In Ref. [7] study of Cases 1 and 2 was briefly reported. The aims of the present section is to recover some of the main results of [7], providing additional details of the dynamics of the wave parameters.

A. Stationary periodic waves. Parametrization

In this and next subsections we recall some known facts from the theory of the NLS equation (9), where without restriction of generality we put $|M| = 1/2$ and define $\tilde{\sigma} = \sigma \text{sign}(M)$ (recovering the general case is provided by evident renormalization):

$$i\psi_t = -\psi_{xx} + 2\tilde{\sigma} |\psi|^2 \psi. \quad (16)$$

We will concentrate on periodic solutions $\psi(x, t) = \psi(x + L, t)$. In physical units the period is recovered to be $a_{\perp} L / \epsilon$, and thus, in accordance with the scaling of the Case 1, $a_{\perp} L / \epsilon \sim \xi \gg \Lambda$. The simplest stationary solutions of such type can be obtained in a form of a standing wave by means of the ansatz

$$\psi(x, t) = e^{i\omega t} u(x) \quad (17)$$

where $u(x)$ is a real periodic function, $u(x) = u(x + L)$, and ω is a frequency of the wave. In this case (16) is

reduced to the ordinary differential equation $-u_{xx} + \omega u + 2\tilde{\sigma} u^3 = 0$ which immediately yields

$$x - x_0 = \int_0^u \frac{du}{\sqrt{C + \omega u^2 + \tilde{\sigma} u^4}}. \quad (18)$$

Here x_0 and C are the integration constants. As far as a stationary solution, $u(x)$, is found, a periodic wave moving with a constant velocity V is obtained as

$$\psi(x, t) = \exp \left[i \left(\omega - \frac{V^2}{4} \right) t + i \frac{V}{2} x \right] u(x - Vt). \quad (19)$$

Next steps depend on a particular choice of the parameters C and ω . It turns out, however, that for our purposes another parametrization, provided by the inverse scattering technique (IST), is more convenient.

B. Some elements of the Inverse Scattering Technique

The starting point of the IST (see e.g. [16] for details) consists of the fact that Eq. (16) appears as a compatibility condition for two systems of differential equations

$$|f\rangle_x = \mathbf{U}|f\rangle, \quad |f\rangle_t = \mathbf{V}|f\rangle \quad (20)$$

where a ket-vector is defined as $|f\rangle = \text{col}(f_1, f_2)$, $f_{1,2} = f_{1,2}(x, t)$, and 2×2 matrices \mathbf{U} and \mathbf{V} are given in Appendix A. The first of systems (20) considered as a spectral problem is referred to as a Zakharov-Shabat (ZS) problem.

Let us introduce a bra-vector $\langle f| = (-f_2, f_1)$ and define the internal product $\langle f|g\rangle = f_1 g_2 - f_2 g_1$, [18], and a projector matrix

$$\mathbf{P} \equiv |f\rangle \langle g| = \begin{pmatrix} -f_1 g_2 & f_1 g_1 \\ -f_2 g_2 & f_2 g_1 \end{pmatrix}. \quad (21)$$

As it is clear, if $|f\rangle$ and $|g\rangle$ are two independent solutions of each of the systems (20), then $\langle f|g\rangle$ is nothing but a Wronskian of each of them, and hence it does not depend neither on x nor on t , i.e. $\langle f|g\rangle = p(\lambda)$, where $p(\lambda)$ is a function of the spectral parameter (introduced in Appendix A). Let us suppose that a solution $|f\rangle = \text{col}(f_1, f_2)$ of (20) with some ψ is given. Then the symmetry properties of the matrices \mathbf{U} and \mathbf{V} imply that also $|g\rangle = \text{col}(\bar{f}_2, \bar{\sigma} \bar{f}_1)$ is a solution of (20) with the same ψ . Using the pair of the solutions $|f\rangle$ and $|g\rangle$ one obtains that $\langle f|g\rangle = \tilde{\sigma} |f_1|^2 - |f_2|^2 = p(\lambda)$ depends only on the spectral parameter.

Next, by straightforward algebra one ensures that \mathbf{P} solves equations

$$\mathbf{P}_x = [\mathbf{U}, \mathbf{P}], \quad \mathbf{P}_t = [\mathbf{V}, \mathbf{P}], \quad (22)$$

from which it follows that

$$\Delta P^2 - 4P_{12}P_{21} = P(\lambda) \quad (23)$$

where $\Delta P = P_{22} - P_{11}$, P_{ij} being entries of the matrix \mathbf{P} , and $P(\lambda)$ is a function of λ only (i.e. does not depend on x and t). For the chosen pair of solutions one verifies that $P_{21} = \tilde{\sigma} \bar{P}_{12}$ and thus $P_{12}P_{21} = \tilde{\sigma}|f_1|^2|f_2|^2$, and $\Delta P = \tilde{\sigma}|f_1|^2 + |f_2|^2$. Consequently, $P(\lambda) = p^2(\lambda)$, i.e. it is a real positive function of λ .

So far we did not specify dependence of $P(\lambda)$ (or $p(\lambda)$) on λ . By imposing such dependence one restricts consideration to a specific class of solutions. We are interested in the simplest periodic ones. To this end we notice that \mathbf{U} and \mathbf{V} are matrix polynomials in λ . This allows one to make a guess that the simplest nontrivial solution $|f\rangle$, and hence \mathbf{P} , should also be searched in forms of polynomials with respect to λ . As far as \mathbf{V} is quadratic with respect to λ , one has to consider $|f\rangle$ to be second (or higher) order polynomial with respect to λ . Since \mathbf{P} is quadratic with respect to the elements of $|f\rangle$ one concludes that the simplest nontrivial form of $P(\lambda)$ must also be a polynomial of the fourth degree with respect to λ :

$$P(\lambda) = (\lambda - \lambda_1)(\lambda - \lambda_2)(\lambda - \lambda_3)(\lambda - \lambda_4) \quad (24)$$

where $\lambda_j (j = 1, \dots, 4)$ are given complex numbers. Then, $\xi_j = \text{Re}\lambda_j$ and $\eta_j = \text{Im}\lambda_j$ can be considered as parameters characterizing respective solutions of the nonlinear problem (16). The requirement for $P(\lambda)$ to be real imposes four constraints on the parameters λ_j , what means that we have only four independent real parameters determining the solution. Indeed, considering $\bar{P}(\lambda)$ one concludes that either (i) all λ_j are real, i.e. all $\eta_j = 0$ and ξ_j parametrize the problem, or (ii) two of them are real and two ones are complex conjugated, say $\text{Im}\lambda_1 = \text{Im}\lambda_2 = 0$ and $\lambda_3 = \bar{\lambda}_4$, then the parameters are $\{\xi_1, \xi_2, \xi_3, \eta_3\}$, or (iii) there are two pairs of complex conjugated parameters, say $\lambda_1 = \bar{\lambda}_2$ and $\lambda_3 = \bar{\lambda}_4$, i.e. the parameters are e.g. $\{\xi_1, \xi_3, \eta_1, \eta_3\}$.

Then one can show (see Appendix B) that there exist the following links among the parameters:

$$\omega = \frac{1}{2} \sum_{\substack{i,j=1 \\ i \neq j}}^4 \lambda_i \lambda_j, \quad (25)$$

$$C = \frac{\tilde{\sigma}}{4} (\omega^2 - \lambda_1 \lambda_2 \lambda_3 \lambda_4) \quad (26)$$

as well as

$$0 = \lambda_1 + \lambda_2 + \lambda_3 + \lambda_4. \quad (27)$$

The last condition leaves us with only two independent parameters.

The Table II summarizes well known analytical expressions for such solutions (hereafter we use the standard notations for the Jacobi elliptic functions $\text{pq}(x, m)$ with $\text{p}=\text{c}, \text{s}, \text{d}$ and $\text{q}=\text{n}, [17]$).

A convenient representation of the results is given by the locations of the parameters λ_j on the Riemann surface of the function $p(\lambda)$, which is shown in Fig.1 (Figs.1

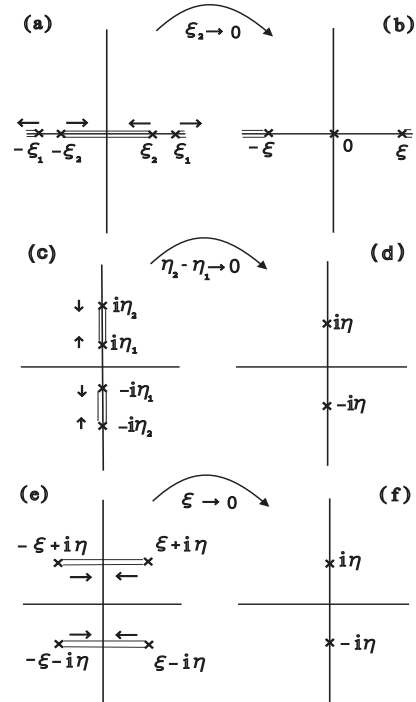


FIG. 1: The Riemann surface of the function $p(\lambda) = \sqrt{P(\lambda)}$ consists of two complex plains, one of which is shown in Figs. (a) for sn-wave: $\lambda_1 = -\lambda_3 = \xi_1$, $\lambda_2 = -\lambda_4 = \xi_2$; (c) for dn-wave: $\lambda_1 = \bar{\lambda}_3 = i\eta_1$, $\lambda_2 = \bar{\lambda}_4 = i\eta_2$; and (e) for cn-wave: $\lambda_1 = -\bar{\lambda}_3 = -\lambda_2 = -\bar{\lambda}_4 = \xi + i\eta$. The right panels show the modification of the Riemann surface subject to the limiting transition $m \rightarrow 1$ shown in the last column of the Table II. The lines connecting the parameters λ_j show cuts of the respective two-sheet Riemann surfaces.

(a), (c), and (e) correspond to the above cases (i), (ii), and (iii)).

Let us now assume that by some means one can provide shifts of the spectral parameters in the complex plane. More specifically, we consider three situations corresponding to collapse of two pairs of the branching points, λ_j , as it is shown by the arrows in Fig.1.

At $\tilde{\sigma} = 1$, subject to transition $\xi_2 \rightarrow 0$ and $\xi_1 \rightarrow \xi = 2\rho$ (Fig.1b) the Riemann surface of $p(\lambda)$ is transformed in the Riemann surface of the spectral parameter of the ZS problem, subject to the so-called finite density boundary conditions for the field ψ : $\lim_{x \rightarrow \pm\infty} \psi = \rho e^{\pm i\varphi}$, where ρ and φ are real constants. Then the passage between (a) and (b) illustrates deformation of the branching points $\xi_{1,2}$ resulting in transformation of the sn-wave into a single dark soliton. The point $\xi_2 = 0$ corresponding to the discrete spectrum of the ZS spectral problem, which determines a static dark soliton, while points $\pm\xi_1 = \pm 2\rho$ are transformed into edges of the continuum spectrum of the ZS spectral problem.

In the case of the NLS equation with $\tilde{\sigma} = -1$ and

TABLE II: The simplest static periodic solutions.

$\tilde{\sigma}$	periodic solution	m	limit $m \rightarrow 0$	limit $m \rightarrow 1$
1	$\psi_{\text{sn}} = e^{i(\xi_1^2 + \xi_2^2)t/2} \frac{\xi_1 - \xi_2}{2} \text{sn} \left(\frac{\xi_1 + \xi_2}{2} x, m \right)$	$\frac{(\xi_1 - \xi_2)^2}{(\xi_1 + \xi_2)^2}$	$e^{i\xi^2 t} \frac{\Delta\xi}{2} \sin(\xi x)$	$\frac{\xi}{2} e^{-i\xi^2 t/2} \tanh \left(\frac{\xi}{2} x \right)$
-1	$\psi_{\text{dn}} = e^{-i(\eta_1^2 + \eta_2^2)t/2} \frac{\eta_1 + \eta_2}{2} \text{dn} \left(\frac{\eta_1 + \eta_2}{2} x, m \right)$	$\frac{4\eta_1\eta_2}{(\eta_1 + \eta_2)^2}$	$\eta e^{-i\eta^2 t}$	$\eta e^{i\eta^2 t} \text{sech}(\eta x)$
-1	$\psi_{\text{cn}} = e^{i(\xi^2 - \eta^2)t/2} \eta \text{cn} \left(\sqrt{\eta^2 + \xi^2} x, m \right)$	$\frac{\eta^2}{\xi^2 + \eta^2}$	$e^{-i\eta^2 t/2} \eta \cos(\eta x)$	$\eta e^{i\eta^2 t} \text{sech}(\eta x)$

zero boundary conditions, $\lim_{x \rightarrow \pm\infty} |\psi| = 0$, bright soliton solutions are determined by the zeros in the upper half-plane of the spectral parameter. If a soliton is static (and this is the case we are considering), the only discrete eigenvalue is placed on the imaginary axis, and is designated $i\eta$ (Figs.1c and d). One can arrive at such plane by shifting the branch points of the dn-wave as it is shown on the passage between Figs.1c and d. The branching points $\eta_{1,2}$ collapse into a point corresponding to the discrete eigenvalue of the ZS spectral problem. Alternatively, one can arrive at a static bright soliton solution, starting with a cn-wave, and providing displacements of the branching points as it is shown by the arrow between Figs.1e and f.

C. BEC with a varying scattering length

As it has been shown above, in order to change the aspect ratio of a periodic wave, and in particular to transform it into a soliton one has to find a way to move accordingly the branching points λ_j , what is the same as to change the wave parameters. It turns out that the limiting transitions shown in Table I and in Fig.1 cannot be reached in practice because they require change of the boundary conditions of the problem and thus change of the number of atoms involved. That is why instead of looking for a possibility of transforming periodic waves in single solitons one can to explore a possibility of their transform in a sequence (we call it train) of solitons equally spaced and thus preserving the period of the wave. This can be done by perturbing the evolution equation, however weakly enough in order to do not destroy the regular structure of the periodic wave, i.e. adiabatically. In particular one can consider either change of the effective mass, by means of the variation of the laser field intensity or geometry of laser beams, or change of the nonlinearity, which in the case of a BEC can be achieved by means of the FR affecting the scattering length and controlled by an external magnetic field $B(t)$ varying with time. In the present paper we will concentrate on the last option. Then a model simulating the

process can be written as follows (see [19]):

$$a_s(t) = a_s(0)g(t), \quad g(t) = \frac{\Delta B(0)(\Delta B(t) + \Delta_{res})}{\Delta B(t)(\Delta B(0) + \Delta_{res})}, \quad (28)$$

where $a_s(0)$ is the initial value of the scattering length, $\Delta B = B(t) - B_0$ is the initial field, B_0 deviation from the resonant value B_0 , and Δ_{res} is the width of the resonance.

Temporal dependence of a_s means the dependence on time of the nonlinear coefficient: $g_0 \rightarrow g_0 \cdot g(t)$. Assuming that dependence of $g(t)$ on time is slow enough (i.e. is governed by $\epsilon^2 \tilde{t}$, where ϵ is given by (2)) one can repeat the arguments of Sec. II, substituting g_0 by $\tilde{g}_0 = g_0 \cdot \tilde{g}(0)$, what results in modification of each of the evolution equations (9) [respectively (16)], (11), (13), and (15), reduced to the modulation of the nonlinearity by the function $g(t)$. In particular (16) now reads

$$i\psi_t + \psi_{xx} - 2\tilde{\sigma}g(t)|\psi|^2\psi = 0. \quad (29)$$

In what follows we consider only the case when $g(t)$ is a positive function, i.e. the FR does not change the type of the two-body interaction. Then, in order to study evolution of the condensate within the framework of the model (29) we notice that substitution

$$\psi(x, t) = \frac{v(x, t)}{\sqrt{g(t)}} = e^{-\zeta(t)/2} v(x, \zeta) \quad (30)$$

where

$$\zeta = \zeta(t) = 2 \int_0^t \gamma(t') dt' = \ln g(t), \quad \zeta(0) = 0 \quad (31)$$

transforms (29) into a dissipative NLS equation (c.f. (16))

$$iv_t + v_{xx} - 2\tilde{\sigma}|v|^2v = i\gamma v \quad (32)$$

where

$$\gamma(t) = \frac{1}{2g(t)} \frac{dg(t)}{dt} = \frac{1}{2} \frac{d\zeta}{dt}. \quad (33)$$

Thus, for slowly varying $g(t)$ the right hand side of Eq. (32) can be considered as a small perturbation:

$|\gamma(t)| \ll 1$. It is to be emphasized here that slow dependence means slow in terms of slow time $\epsilon^2 \tilde{t}$, what is satisfied, for example by the function g depending on $\epsilon^{5/2} \tilde{t}$. If the nonlinearity increases ($\gamma(t) > 0$, the case we will deal with) then the perturbation describes growth, otherwise, when the nonlinearity is decaying ($\gamma(t) < 0$) the perturbation in (32) describes dissipation.

Since $g(t)$ has been introduced such that $g(0) = 1$ it follows from Eq. (30), that $v(x, 0) = \psi(x, 0)$.

D. Adiabatic approximation

Under influence of the dissipative perturbation a wave shape is changed what can be described by variations of the parameters λ_j assuming them to be slow functions of time t (the so-called *adiabatic approximation*). Equations which govern their evolution can be derived by the following simple method.

First of all we recall that in all the examples considered in Sec. III the waves were two-parametric and hence we expect to obtain two equations of the adiabatic approximation. Since the coefficients in the dissipative model (32) are supposed to be independent on x , the perturbation does not result in change of the period L of the nonlinear wave what can be expressed as follows

$$\frac{d}{d\zeta} L(\lambda_1, \lambda_2) = 0. \quad (34)$$

Here we temporarily change notations and use $\lambda_{1,2}$ for two parameters of a periodic solution: thus $\lambda_{1,2} = \xi_{1,2}$ for the sn-wave, $\lambda_{1,2} = \eta_{1,2}$ for the dn-wave, and $\lambda_1 = \eta$ and $\lambda_2 = \xi$ for the cn-wave.

Next it is a straightforward algebra to show that the integral

$$N = \int_0^L |v|^2 dx \quad (35)$$

of a periodic solution of (32) (below it will be referred to as a number of particles, assuming that there is no confusion with a real number of particles given by \mathcal{N}) evolves according to

$$\frac{dN(\lambda_1, \lambda_2)}{d\zeta} = N(\lambda_1, \lambda_2). \quad (36)$$

Then, if the expressions for L and N in terms of $\lambda_{1,2}$ are known, Eqs. (34) and (36) reduce to a system of two first order differential equations for $\lambda_{1,2}$. The form of this system depends, of course, on the choice of the initial periodic distribution.

E. sn-wave in a BEC with $a_s M > 0$

We start with the adiabatic dynamics of a periodic matter wave in a BEC with $\bar{\sigma} = 1$ and look for a solution

of (32) in a form given in the first row of Table II and compute

$$L = \frac{8K(m)}{\xi_1 + \xi_2}, \quad N = 2(\xi_1 + \xi_2)[K(m) - E(m)] \quad (37)$$

where $K(m)$ and $E(m)$ are standard notation for the complete elliptic integrals of the first and second kinds, respectively [17, 20]. Now, considering ξ_j as functions of time, or more precisely of $\zeta = \zeta(t)$ and substituting (37) into (34) and (36) we obtain

$$\begin{aligned} \frac{d\xi_1}{d\zeta} &= \frac{\xi_1(\xi_1 + \xi_2)[K(m) - E(m)]}{2\xi_1 K(m) - (\xi_1 + \xi_2)E(m)}, \\ \frac{d\xi_2}{d\zeta} &= \frac{\xi_2(\xi_1 + \xi_2)[K(m) - E(m)]}{2\xi_2 K(m) - (\xi_1 + \xi_2)E(m)} \end{aligned} \quad (38)$$

where m is defined through ξ_j in Table II.

For the sake of definiteness we assume that the parameters ξ_j are chosen such that initially $\xi_{01} > \xi_{02}$ (hereafter $\xi_{0j} = \xi_j(t=0)$), i.e. initially they are located as it is shown in Fig.1a. Then one immediately concludes that $d\xi_1/d\zeta > 0$, i.e. ξ_1 is a monotonically growing function of time. One can also show (see Appendix C) that ξ_2 is a monotonically decreasing function and thus $m \rightarrow 1$ as time goes to infinity. To describe the respective limiting behavior we employ the well known asymptotics of the elliptic integrals (C1), and reduce (38) in the leading order (when $\xi_1 \rightarrow \infty$ and $\xi_2 \rightarrow 0$) to

$$\frac{d\xi_1}{d\zeta} = \frac{\xi_1}{2}, \quad \frac{d\xi_2}{d\zeta} = -\frac{\xi_2}{2} \ln \frac{\xi_1}{\xi_2}. \quad (39)$$

The first of these equations is trivially solved. To solve the second one we observe that from (39) one deduces

$$\frac{d\xi_2}{d\xi_1} = -\frac{\xi_2}{\xi_1} \ln \frac{\xi_1}{\xi_2} \quad (40)$$

which is also readily solved giving

$$\xi_2 = \exp(1 + \ln \xi_1 + C_0 \xi_1) \sim e^{C_0 \xi_1}.$$

Here C_0 is an integration constant, which can be found from the (asymptotic) condition of the period conservation computed from (37): $L \sim \frac{4}{\xi_1} \ln \frac{\xi_1}{\xi_2} \sim -4C_0$. Then we arrive at the asymptotics:

$$\xi_1 \sim e^{\zeta/2}, \quad \xi_2 \sim \xi_1 e^{-L\xi_1/4}. \quad (41)$$

Thus one observes a scenario different from one shown in Fig.1a,b and corresponding to the deformation of a periodic sn-wave to a single dark soliton (see the example in Fig.2b, below). Namely, now ξ_1 goes to the infinity and we obtain a ‘‘train of dark solitons’’. This is related to the fact that the perturbation does not affect the period of the nonlinear wave, while in order to obtain a single dark soliton the period should go to the infinity in the process of the wave deformation. Meantime, the shape of the train of dark solitons indeed approximates to a shape of a set of static dark solitons, what occurs due to extremely rapid convergence of ξ_2 to zero, what is illustrated in inset in Fig.2b.

F. dn-wave in a BEC with $a_s M < 0$

Let us now turn to the case $\tilde{\sigma} = -1$, and consider deformations of the periodic dn-wave, given by second row in Table II, resulting in a train of bright solitons (the counterpart of the transformation shown in Figs.1c,d). The period L and the number of particles N are now given by

$$L = \frac{4K(m)}{\eta_1 + \eta_2}, \quad N = (\eta_1 + \eta_2)E(m). \quad (42)$$

Assuming that parameters η_j depend on time and substituting (42) in (34) and (36) we obtain a system of the equations of the adiabatic approximation for η_1 and η_2 :

$$\begin{aligned} \frac{d\eta_1}{d\zeta} &= \frac{\eta_1(\eta_1 + \eta_2)E(m)}{(\eta_1 + \eta_2)E(m) + (\eta_1 - \eta_2)K(m)}, \\ \frac{d\eta_2}{d\zeta} &= \frac{\eta_2(\eta_1 + \eta_2)E(m)}{(\eta_1 + \eta_2)E(m) - (\eta_1 - \eta_2)K(m)} \end{aligned} \quad (43)$$

where m is given in Table II, ζ is defined by Eq. (31), and for the sake of definiteness it is supposed that $\eta_2 > \eta_1$.

Like in the previous subsection one can show that the both η_j are monotonically increasing functions (see Appendix C). Moreover, it is evident that η_2 growth more rapidly than η_1 . To consider the limit $|\eta_1 - \eta_2| \rightarrow 0$, i.e. at $m \rightarrow 1$, we introduce $\eta = (\eta_1 + \eta_2)/2$ and $\Delta\eta = |\eta_1 - \eta_2|/2$. Then using (C1) we obtain from (43):

$$\frac{d\eta}{d\zeta} = \eta, \quad \frac{d\Delta\eta}{d\zeta} = -\Delta\eta \ln \frac{\eta}{\Delta\eta}. \quad (44)$$

Comparing these equations with (39) one observes the *universality* of the limiting behavior. Thus using (41) one immediately writes down the asymptotic formulas (as in the previous case the constant is found from the conservation of the wave period)

$$\eta \sim e^\zeta, \quad \Delta\eta \sim \eta e^{-L\eta/4}. \quad (45)$$

Like in the case of the sn-wave, there is a peculiarity of the behavior of the dn-wave parameters in the limit $m \rightarrow 1$: the both η_1 and η_2 tend to infinity (see the inset in Fig.6a, below), what is consistent with the fact that keeping the wave period to be a constant one cannot obtain a single bright soliton. Meantime, as we could expect the difference $|\eta_1 - \eta_2|$ rapidly goes to zero, what results in approaching of the wave shape to the shape of a ‘‘train of bright solitons’’ (see the example in Fig.6a).

G. cn-wave in a BEC with $a_s M < 0$

Finally, we consider the case of a cn-wave (the third line of Table II) in a BEC with $\tilde{\sigma} = -1$. The period and the number of particles of the cn-wave are now given by

$$L = \frac{4K(m)}{\sqrt{\xi^2 + \eta^2}}, \quad N = 4\sqrt{\xi^2 + \eta^2}E(m) - \xi^2 L. \quad (46)$$

Substitution these expressions into Eqs. (34) and (36) yields

$$\begin{aligned} \frac{d\eta}{d\zeta} &= \frac{[(\eta^2 + \xi^2)E(m) - \xi^2 K(m)]E(m)\eta}{\eta^2 E^2(m) + \xi^2 [K(m) - E(m)]^2}, \\ \frac{d\xi}{d\zeta} &= \frac{[\xi^2 K(m) - (\eta^2 + \xi^2)E(m)][K(m) - E(m)]\xi}{\eta^2 E^2(m) + \xi^2 [K(m) - E(m)]^2}. \end{aligned} \quad (47)$$

Now η and ξ are respectively increasing and decreasing functions. As in the two previous examples analytical treatment can be given for the limiting case, which is now $\xi \rightarrow 0$ and $\eta \rightarrow \infty$. Using (C1) it is a straightforward algebra to ensure that in the case at hand we arrive at already known equations of motion

$$\frac{d\eta}{d\zeta} = \eta, \quad \frac{d\xi}{d\zeta} = -\xi \ln \frac{\eta}{\xi} \quad (48)$$

and thus to the *universal* law of the limiting transition (c.f. (41) and (45))

$$\eta \sim e^\zeta, \quad \xi \sim \eta e^{-L\eta/4}. \quad (49)$$

Dynamics of respective parameters η and ξ on time is shown in inset in Fig.4b.

IV. BEC SUBJECT TO FR IN A PERIODIC POTENTIAL WITH LARGE PERIOD

A. Stationary solution and adiabatic approximation

The Case 1 from the Table I is the simplest one since it deals with the integrable NLS equation (9). It turns out that the Case 3 from Table I with varying nonlinearity can also be treated within the framework of the adiabatic perturbation theory, due to the fact that some solutions of the NLS equation with a constant nonlinearity are known explicitly. They were considered in details in Refs. [21] and are partially summarized in the present subsection.

To this end we notice that the ansatz (17) now results in the stationary equation

$$u_{xx} = (\omega + U(x) + 2\tilde{\sigma}u^2)u, \quad (50)$$

which allows one to construct a lattice potential $U(x)$, in an explicit form, when a stationary periodic solution of the NLS equation (16), which will be written down as $\psi = e^{i\omega t}u_0(x)$, is known. Indeed, one can easily verify, that the function $\psi = e^{i\omega t}\tilde{u}(x)$ with $\tilde{u}(x) = \sqrt{\chi}u_0(x)$, $\chi > 0$, solves (13) with a periodic potential $U(x) = 2\tilde{\sigma}(1 - \chi)|u_0(x)|^2$. Alternatively, from Eq. (50) one can find a lattice potential $U(x)$ for given wave field $u_0(x)$, subject to the requirement of a regular behavior of $u_{0,xx}/u_0$: $U(x) = \frac{u_{0,xx}}{u_0} - \omega - 2\tilde{\sigma}u_0^2$. By any of the above methods, one can verify that the Jacobi elliptic functions

$pq(\kappa x, m)$, where $p=c,s$ or d , and $q = n$ (more generally one can consider, say, $u_{pq}(x) = (A pq^\beta(\kappa x, m) + B)^\alpha$ with $B > |A|$, α and β being real integers), subject to proper choice of $\tilde{\sigma}$, give the lattice potential

$$U(x) = U_0 \text{sn}^2(\kappa x, m), \quad (51)$$

where U_0 is a positive constant and we returned to the parametrization given by κ and m . (Although one can continue using λ_j , the latter now loose their meaning in the context of the IST.) The respective solutions are summarized in the Table III.

TABLE III: Solutions of the type $(u_{pq}(x, t) = \sqrt{A} pq(\kappa x, m))$. The parameters in the second column have to be chosen to ensure $A > 0$.

pq	$A > 0$	ω
sn	$(\kappa^2 m - U_0/2)\tilde{\sigma}$	$-\kappa^2(1+m)$
cn	$(U_0/2 - \kappa^2 m)\tilde{\sigma}$	$\kappa^2(2m-1) - U_0$
dn	$(U_0/2m - \kappa^2)\tilde{\sigma}$	$\kappa^2(2-m) - U_0/m$

If the nonlinearity depends on time, we again make use of the substitution (30) leading to the equation [c.f. (32)]

$$iv_t + v_{xx} - U_0 \text{sn}^2(\kappa x, m)v - 2\tilde{\sigma}|v|^2v = i\gamma v. \quad (52)$$

As above the right hand side of Eq. (52) is considered as a small perturbation: $|\gamma(t)| \ll 1$. Then, in accordance with the adiabatic approximation, the parameters κ and m will be considered as slow functions of time t , and respectively will be designated as $\tilde{\kappa}$ and \tilde{m} . The equations of their evolution are obtained in the same way as we obtained above the equations for the dependence of $\lambda_{1,2}$ on time. More specifically, they are Eqs. (34), (36), where the period now coincides with the period of the periodic potential, and L and N are expressed through $\tilde{\kappa}$ and \tilde{m} : $L = L(\tilde{\kappa}, \tilde{m})$, $N = N(\tilde{\kappa}, \tilde{m})$. As it is clear the new time-dependent parameters must satisfy initial conditions as follows

$$\tilde{m}(0) = m, \quad \tilde{\kappa}(0) = \kappa \quad (53)$$

where respective links between m and κ are given in the Table III.

B. BEC with a positive scattering length: sn-wave

Let us start with adiabatic dynamics of a periodic matter wave in a BEC with positive scattering length ($\tilde{\sigma} = 1$) and respectively $2\kappa m > U_0$, loaded in the OL (51). Substituting solution for sn-wave (the first row of Table III):

$$v_{\text{sn}} = \sqrt{\tilde{\kappa}^2 \tilde{m} - \frac{U_0}{2}} e^{-i\tilde{\kappa}^2(1+\tilde{m})t} \text{sn}(\tilde{\kappa}x, \tilde{m}) \quad (54)$$

into (52) one obtains:

$$L = \frac{4K(\tilde{m})}{\tilde{\kappa}}, \quad N = \frac{4\tilde{\kappa}^2 \tilde{m} - 2U_0}{\tilde{\kappa} \tilde{m}} [K(\tilde{m}) - E(\tilde{m})]. \quad (55)$$

Now one can distinguish two different situations, where maxima of the atomic density are located in (i) maxima ($U_0 > 0$) and (ii) minima ($U_0 < 0$) of the periodic potential (the examples are shown in Fig.2 (a) and (c), respectively). It is interesting to notice that, although the last situation allows the limit $\tilde{m} \rightarrow 0$, where the distribution is transformed into a sine-wave: $v_{\text{sn}} \rightarrow \sqrt{|U_0|/2} e^{-i\tilde{\kappa}^2 t} \sin(\tilde{\kappa}x)$, it does not allow transition to the linear limit in the sense of a small amplitude, the latter being possible only if $U_0 > 0$ and corresponding to $\tilde{m} \rightarrow U_0/(2\tilde{\kappa}^2)$, which however is not a sine-wave.

For the next step we substitute (55) into (34) and (36), what gives

$$\begin{aligned} \frac{d\tilde{\kappa}}{d\zeta} &= \frac{\tilde{\kappa}(2\tilde{\kappa}^2 \tilde{m} - U_0)}{\Delta_{\text{sn}}} \\ &\quad \times [E(\tilde{m}) - K(\tilde{m})] [E(\tilde{m}) - \tilde{m}'K(\tilde{m})], \quad (56) \\ \frac{d\tilde{m}}{d\zeta} &= \frac{2\tilde{m}\tilde{m}'(2\tilde{\kappa}^2 \tilde{m} - U_0)}{\Delta_{\text{sn}}} K(\tilde{m}) [E(\tilde{m}) - K(\tilde{m})], \end{aligned}$$

where standard notation $\tilde{m}'(\zeta) \equiv 1 - \tilde{m}(\zeta)$ is used and

$$\begin{aligned} \Delta_{\text{sn}} &= U_0 [E^2(\tilde{m}) - \tilde{m}'K^2(\tilde{m})] \\ &\quad + 2\tilde{\kappa}^2 \tilde{m} \left\{ [E(\tilde{m}) - K(\tilde{m})]^2 - \tilde{m}K^2(\tilde{m}) \right\}. \end{aligned}$$

The obtained system can be analyzed in limiting cases. We start with the ‘‘linear’’ limit at $U_0 < 0$, by imposing the initial conditions

$$\tilde{m}(0) = 0, \quad \tilde{\kappa}(0) = \kappa = 2\pi/L \quad (57)$$

(the case becomes trivial in absence of the periodic potential, when $U_0 = 0$). Using the asymptotics (C2) and condition $\tilde{m} \ll 1$ we obtain from (55)

$$\frac{\tilde{\kappa}}{\kappa} = 1 + \frac{\tilde{m}}{4}. \quad (58)$$

Next, requiring $2\tilde{\kappa}^2 \tilde{m} \ll |U_0|$, what for $\kappa \sim 1$ is equivalent to $|\tilde{\kappa} - \kappa| \ll U_0$, we deduce from the first of the equations (56)

$$\tilde{\kappa}^2 \approx \kappa^2 \left(1 + \frac{4|U_0|\zeta}{16\kappa^2 + |U_0|} \right) \quad (59)$$

where we used the condition $4U_0^2\zeta \ll 1$, necessary for the smallness of \tilde{m} . Thus with time $\tilde{\kappa}$ grows and \tilde{m} approaches the unity.

In the opposite limit $\tilde{m} \rightarrow 1$ one can use the asymptotics (C1) to obtain

$$\tilde{\kappa} \sim e^{\zeta/2}, \quad \tilde{m} = 1 - e^{-L\tilde{\kappa}/2}. \quad (60)$$

Now the potential amplitude does not affect the asymptotics in the leading order. This is expectable behavior

because it corresponds to large particle densities, when two body interactions dominate the effect of the periodic potential.

In Fig.2 we show examples of numerical solutions of the equations of the adiabatic approximation for three different situations with respect to U_0 and intermediate values of the wave parameters. In all the cases the wave is transformed in a sequence of dark solitons. The external potential affects the velocity of the process.

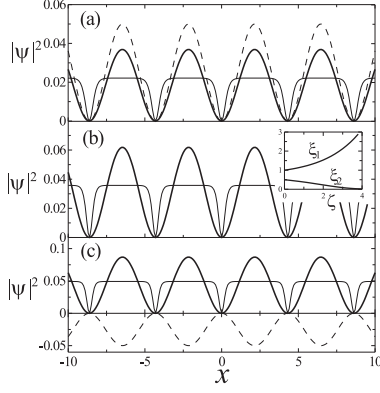


FIG. 2: Examples of sn-wave solutions at $\zeta = 0$ (solid thick lines) and $\zeta = \zeta_{fin}$ (solid thin lines) in the periodic potential (51) (dashed lines) for (a) $U_0 = 0.05$, and $\zeta_{fin} = 5$; (b) $U_0 = 0$, $\zeta_{fin} = 6$, and (c) $U_0 = -0.05$, $\zeta_{fin} = 6$. The inset shows dynamics of the parameters ξ_1 and ξ_2 , which connection with \tilde{m} and $\tilde{\kappa}$ is given in Table II and is obtained by solving numerically (56). In all the cases $m = 0.11$ and $\kappa = 0.75$.

C. BEC with a negative scattering length: cn-wave

Let us now consider deformation of a periodic cn-wave resulting in creation of a train of bright matter solitons in a BEC with the negative scattering length, $\tilde{\sigma} = -1$, loaded in the OL (51). The cn-wave unaffected by FR is given by the second row of the Table III:

$$v_{cn} = \sqrt{\tilde{\kappa}^2 \tilde{m} - \frac{U_0}{2}} e^{i(\tilde{\kappa}^2(2\tilde{m}-1) - U_0)t} \text{cn}(\tilde{\kappa}x, \tilde{m}). \quad (61)$$

Notice that, as above, choice of the magnitude of the OL amplitude has the only constrain $U_0 < 2\tilde{\kappa}^2 \tilde{m}$. However, unlike in the previous case of sn-wave, now the value of the amplitude of the OL changes not only the initial atomic distribution but also the frequency of the solution.

Now we have

$$\begin{aligned} L &= \frac{4K(\tilde{m})}{\tilde{\kappa}^2 \tilde{m}}, \\ N &= \frac{4\tilde{\kappa}^2 \tilde{m} - 2U_0}{\tilde{\kappa} \tilde{m}} [E(\tilde{m}) - \tilde{m}'K(\tilde{m})] \end{aligned} \quad (62)$$

and equations of the adiabatic approximation (34), (36) can be written down in the form:

$$\begin{aligned} \frac{d\tilde{\kappa}}{d\zeta} &= \frac{\tilde{\kappa}(2\tilde{\kappa}^2 \tilde{m} - U_0)}{\Delta_{cn}} [E(\tilde{m}) - \tilde{m}'K(\tilde{m})]^2, \\ \frac{d\tilde{m}}{d\zeta} &= \frac{2(2\tilde{\kappa}^2 \tilde{m} - U_0)\tilde{m}\tilde{m}'}{\Delta_{cn}} K(\tilde{m}) [E(\tilde{m}) - \tilde{m}'K(\tilde{m})] \end{aligned} \quad (63)$$

where

$$\begin{aligned} \Delta_{cn} &= U_0 [E^2(\tilde{m}) - \tilde{m}'K^2(\tilde{m})] \\ &+ 2\tilde{\kappa}^2 \tilde{m} \{E^2(\tilde{m}) + \tilde{m}'K(\tilde{m}) [K(\tilde{m}) - 2E(\tilde{m})]\}. \end{aligned}$$

As before we consider the limiting cases starting with the initial conditions (57) what is possible only for negative U_0 . The link (58) holds in the case at hand, while the dynamics of $\tilde{\kappa}$ is governed by the formula

$$\tilde{\kappa}^2 \approx \kappa^2 \left(1 + \frac{4|U_0|\zeta}{16\kappa^2 - |U_0|}\right). \quad (64)$$

The obtained result reveals an interesting feature: depending on the amplitude of the potential barrier between two adjacent minima, U_0 , the amplitude of the periodic wave is either increasing, if $-16\kappa^2 < U_0 < 0$, or decreasing, if $U_0 < -16\kappa^2$. This is a general property, rather than the phenomenon observed in the limit of small \tilde{m} . Indeed, in Fig.3 we show various examples of the dependence of U_0 on the parameter \tilde{m} at which Δ_{cn} in the denominators of the adiabatic equations (63) acquires zero value. Since the numerators in (63) are positive above (below) the respective curves, \tilde{m} and $\tilde{\kappa}$ are increasing (decreasing), while in small vicinities of each of the curves, where Δ_{cn} is close to zero the adiabatic approximation in the form (63) is not valid.

To explain the described behavior we notice that decreasing of the wave amplitude is possible only for negative U_0 . In the case under consideration, where $U_0 < 0$, atoms are collected around maxima of the potential (what happens due to attractive interactions and is impossible in the linear limit). Thus the condensate undergoes the effect of two forces acting in opposite directions: one originated by attractive interaction among particles and another force, tempting to separate condensates, due to the lattice potential. When the height of the potential barrier becomes larger than some critical value, U_{cr} , the second force becomes dominant, and the condensate tends to “split” in the vicinity of each maxima resulting in decrease of the amplitude and shift of the atomic density toward the potential minima (notice, that this situation reminds the case depicted in Fig.2a).

Returning to the asymptotic (64) we observe that \tilde{m} becomes negative if $U_0 < -16\kappa^2$ and thus the atomic density is approximated by the function

$$\begin{aligned} v_{cn} &= \sqrt{\frac{|U_0|}{2} - \tilde{\kappa}^2 |\tilde{m}|} e^{i(-\tilde{\kappa}^2(2|\tilde{m}|+1) + |U_0|)t} \\ &\times \text{cd} \left(\sqrt{1 + |\tilde{m}|} \tilde{\kappa}x, \frac{|\tilde{m}|}{1 + |\tilde{m}|} \right). \end{aligned} \quad (65)$$

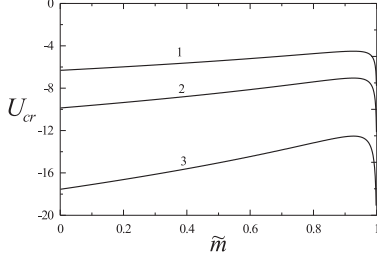


FIG. 3: Dependence of the U_{cr} vs \tilde{m} obtained from the condition $\Delta_{cn} = 0$ for different values of period L (curves 1, 2, and 3 correspond to $L = 10, 8,$ and 6).

When the amplitude of the periodic wave growth, i.e. when $-16\kappa^2 < U_0 < 2\kappa^2 m$ one observes generation of the train of bright solitons. An example of numerical solutions of equation of the adiabatic approximation for different intensities of periodic potential is presented in Fig.4.

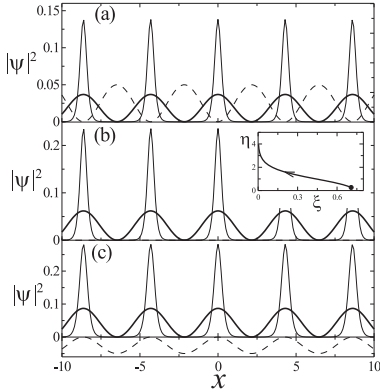


FIG. 4: Examples of cn-wave solutions at $\zeta = 0$ (solid thick lines) and $\zeta = \zeta_{fin}$ (solid thin lines) in the periodic potential (dashed lines) for (a) $U_0 = 0.05$, and $\zeta_{fin} = 4.5$; (b) $U_0 = 0$, $\zeta_{fin} = 4$, and (c) $U_0 = -0.05$, $\zeta_{fin} = 3.5$. The inset in (b) shows dynamics of the parameters η and ξ given by (63). In all cases $m = 0.11$ and $\kappa = 0.75$.

D. BEC with a negative scattering length. dn-wave

As the last example of the adiabatic dynamics we consider evolution of the periodic dn-wave. As in the previous case the attractive nature of the interaction ($\tilde{\sigma} = -1$) and application of the FR result in creation of a train of bright matter solitons in a BEC placed in the OL. A solution of (52) is searched now in the form (see last row

of the Table III)

$$v_{dn} = \sqrt{\left(\tilde{\kappa}^2 - \frac{U_0}{2\tilde{m}}\right)} e^{i(\tilde{\kappa}^2(2-\tilde{m})-U_0/\tilde{m})t} \text{dn}(\tilde{\kappa}x, m) \quad (66)$$

for which

$$L = \frac{2K(\tilde{m})}{\tilde{\kappa}}, \quad N = \frac{2(2\tilde{\kappa}^2\tilde{m} - U_0)E(\tilde{m})}{\tilde{\kappa}\tilde{m}} \quad (67)$$

and equations of the adiabatic approximation have the form:

$$\begin{aligned} \frac{d\tilde{\kappa}}{d\zeta} &= \frac{\tilde{\kappa}(2\tilde{\kappa}^2\tilde{m} - U_0)}{\Delta_{dn}} E(\tilde{m}) [E(\tilde{m}) - \tilde{m}'K(\tilde{m})], \\ \frac{d\tilde{m}}{d\zeta} &= \frac{2(2\tilde{\kappa}^2\tilde{m} - U_0)\tilde{m}\tilde{m}'}{\Delta_{dn}} E(\tilde{m})K(\tilde{m}) \end{aligned} \quad (68)$$

where

$$\begin{aligned} \Delta_{dn} &= U_0 [E^2(\tilde{m}) + \tilde{m}'K^2(\tilde{m})] \\ &+ 2\tilde{\kappa}^2\tilde{m} [E^2(\tilde{m}) - \tilde{m}'K^2(\tilde{m})]. \end{aligned}$$

As in the previous case we fix the period of the wave $L(m, \kappa)$ and solving equation $\Delta_{dn} = 0$, find the critical value, U_{cr} for the potential barrier below (above) which the adiabatic equations give the decay (growth) of the wave amplitude with time (see Fig.5).

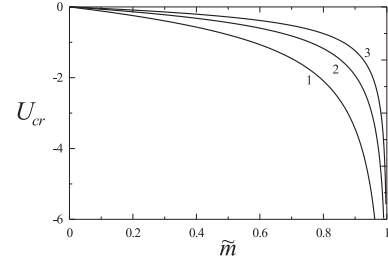


FIG. 5: Dependence of the U_{cr} vs \tilde{m} obtained from the condition $\Delta_{dn} = 0$ for different values of period L (curves 1, 2, and 3 correspond to $L=6, 8,$ and 10).

An example dynamics of the dn-wave obtained by numerical solution of the system (68) is shown in Fig.6.

V. BEC IN AN OL SUBJECT TO FR. INCLUDING BOUNDARY EFFECTS

In the last two sections we considered two situations, described by equations (9) [or (16)] and (13), where the parabolic trap is long enough in the axial direction and dynamics of the BEC can be treated within the framework of the adiabatic theory. In other two cases [Eqs. (11) and (15)] numerical analysis has to be employed. This rises the problem of a choice of adequate initial conditions (i.e. the initial conditions which in the absence of

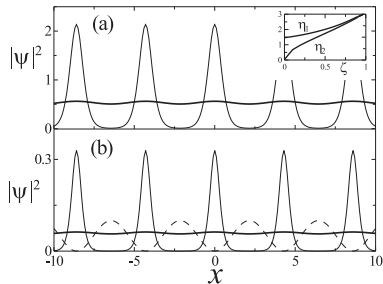


FIG. 6: Examples of dn-wave solutions at $\zeta = 0$ (solid thick lines) and $\zeta = \zeta_{fin}$ (solid thin lines) in the periodic potential (dashed lines) for (a) $U_0 = 0$, and $\zeta_{fin} = 0.25$; (b) $U_0 = 0.1$, $\zeta_{fin} = 3$. The inset in (a) shows the respective dynamics of parameters $\eta_{1,2}$ given by (43). In all cases $m = 0.11$ and $\kappa = 0.75$.

FR are stationary solutions, such that the whole dynamics is originated by the FR only). Case 2, i.e. the NLS equation with an effective mass (11), was studied in [7]. In the present section we are concerned with the Case 4.

To this end, following [4] we impose the following temporal behavior of the nonlinearity

$$g(t) = \exp(t/\tau) \quad (69)$$

where τ is a constant. Then wave evolution is governed by the equation (c.f. (15))

$$i\psi_t = -\psi_{xx} + U_0 \text{sn}^2(\kappa x, m)\psi + 2\tilde{\sigma}e^{t/\tau}|\psi|^2\psi + \nu^2 x^2 \psi. \quad (70)$$

In all numerical simulations reported below, we have supposed that initial scattering length, $a_s(0)$ is small enough, such that the two-body interactions are negligible. This implies smallness of the renormalized density, $|\psi|^2 \ll 1$. The aspect ratio in numerical studies reported below is considered to be $\nu \sim 10^{-3} \div 10^{-4}$. These two facts has allowed us to consider the initial distributions in a form of a modulated wave: $\psi(x, t = 0) = \exp(-\nu x^2/2)u_{\text{pq}}(x)$.

1. Deformation of a cn-wave

First we consider deformation of a periodic cn-wave resulting in creation of a train of bright solitons in a BEC with negative scattering length, $\tilde{\sigma} = -1$, embedded in the OL (51). A typical example of numerical solution of Eq.(70) with initial condition taken in a form a modulated cn-wave is presented in Fig.7. We show two subsequent regimes. First on the time interval $0 \leq t \leq 19$ the FR was switched on and after that at $19 < t \leq 60$ all potentials and FR were switched off, and the condensate was allowed to expand freely.

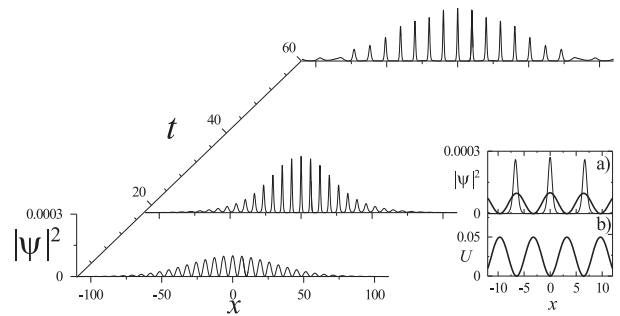


FIG. 7: Dynamics of the cn-wave. In the inset (a) thick and thin lines show initial ($t = 0$) and intermediate ($t = 19$) profiles of the wave, respectively, and in (b) the potential is shown. The parameters are $\nu = 0.0005$, $\tau = 2$, $\kappa = 0.5$, $m = 0.1$, and $U_0 = 0.05$.

From inset (a) in Fig.7 one can see that growth of the scattering length leads to sharpening of peaks of the distribution and to increase of their amplitudes. At an intermediate moment of time (here $t = 19$) we obtain strongly pronounced train of pulses, which is naturally to associate with bright solitons. Strictly speaking the concept of a soliton is mathematically well defined in 1D integrable systems, like NLS equation (9), where each solution is associated with an eigenvalue of discrete spectrum of the ZS spectral problem. In order to use this mathematical definition in our case, we reformulate it in the following way. Let us assume that the evolution in the interval $0 < t < t_0$ for some t_0 is considered. Then we, assume that at t_0 , the trap and lattice potentials are switched off and the output pulse, i.e. one at $t = t_0$, will be governed by the unperturbed NLS equation and split out in a set of solitons (if any). It is this sense in which we understand the statement that at t_0 as number of solitons is created. Respectively, to compute them, we propagate pulse affected by the FR till $t = t_0$, and substitute the output $\psi(x, t = t_0)$ into ZS spectral problem.

The result of this approach applied to the case depicted in Fig.7 is shown in Fig.8, where one can see that initial cn-wave does not have solitons while with increasing the nonlinear coefficient with time the number of solitons starts to grow exponentially (to compute the number of solitons we used the numerical approach due to [23]).

In order to visualize the above approach in Fig.7 we show how the localized pulses created due to the FR propagate after all potentials are switched off at $t = 19$. In Fig.7 we can see that indeed the condensate consists of a set of solitary pulses propagating outwards the center without significant changes of their shapes. This behavior supports the fact that we indeed generated train of bright solitons. Meantime it should be mentioned that at $t = 19$ the number of solitons calculated by solving spectral problem exceeds the number of solitons visible in Fig.7. This can be explained by the facts that peaks in Fig.7 can present bound states consisting of several solitons which move with the same velocities and by the

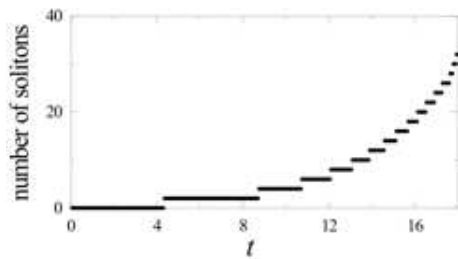


FIG. 8: Dynamics of the number of solitons from the Fig.7. On each time step ($\Delta t = 0.005$) in the interval $0 < t \leq 19$ the function $\psi(x, t)$ considered as an initial condition ψ_n for the respective NLS equation.

fact that small amplitudes solitons cannot be viewed.

2. Deformation of a dn-wave

Now we consider deformation of the dn-wave resulting in creation of a train of bright matter solitons in a BEC with the negative scattering length, $\tilde{\sigma} = -1$. We solve Eq. (70) with initial condition taken as a dn-wave (third row in Table III) modulated by the Gaussian background. As in the previous case, increasing the strength of the inter-particle interactions by means of FR, results in growth and compression of the distribution picks, transforming them in a train of bright solitons (see the insert in Fig.9).

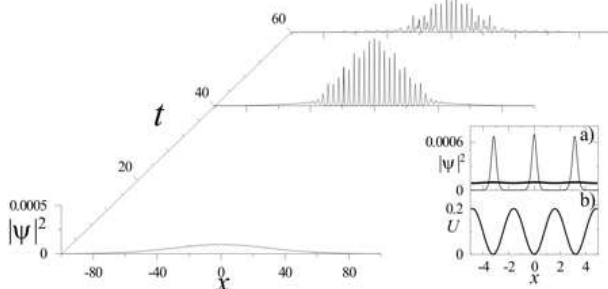


FIG. 9: Dynamics of the dn-wave. In the inset (a) thick and thin lines show initial ($t = 0$) and intermediate ($t = 40$) profiles of the wave which are affected by FR and in (b) the potential is shown. Parameters are $\nu = 0.0005$, $\tau = 4$, $\kappa = 1$, $m = 0.1$, and $U_0 = 0.2$.

In contrast to the previous case, however, in the case of dn-wave the generated train of solitons is not robust, and is destroyed after some time of free propagation, corresponding in Fig.9 to time interval $t > t_0$ where the wave propagates freely. The difference in the behavior of trains of solitons can be understood if one take into account that the dn-wave has a period of the lattice potential while cn-wave has a double period. As a result all bright solitons generated from the dn-wave are in-phase, while solitons generated from cn-wave have alternating phases

(and thus the nearest neighbors are out-of-phase).

3. Deformation of a sn-wave

As a last example of this section we consider the generation of dark solitons in the repulsive case ($\tilde{\sigma} = 1$) of BECs with initial condition taken in a form of a sn-wave (the first row of Table III) modulated by the Gaussian background. This case is very different from the two previous ones. The main reason is that now we are dealing with the periodic wave deformation in a train of dark solitons, which exist against a background, the later affecting soliton properties. Either by change of the nonlinearity or by allowing free expansion of the condensate the background is strongly affected, what becomes an obstacle for numerical (and experimental) realization of the scenario described in the subsection III E. It turns however that it is possible to reduce the effect of the condensate expansion. To this end we use the following arguments.

We start with the NLS equation with constant nonlinear coefficient ($g = 1$)

$$i\partial_t\psi = -\partial_x^2\psi + \nu^2x^2\psi + 2|\psi|^2\psi, \quad (71)$$

and consider stationary solution $\psi = u_{TF}(x)e^{-i\mu t}$ in the Tomas-Fermi approximation, where the gradient term $\partial_x^2\psi$ is neglected: $|u_{TF}|^2 = (\mu - \nu^2x^2)/2$.

Let us assume now that FR is switched on and try to compensate growth of the nonlinearity by a time dependence of the chemical potential $\mu(t)$. Then the respective solution is approximated by $\tilde{\psi} = \tilde{u}_{TF}(x)e^{-i\mathcal{M}(t)}$. In order to compensate the change of the nonlinear part we vary in time the strength of the parabolic potential $\nu \rightarrow \tilde{\nu}(t)$. This substitution into NLS equation in Tomas-Fermi approximation gives $|\tilde{u}_{TF}|^2 = \frac{\mathcal{M}_t - \tilde{\nu}^2(t)x^2}{2g(t)}$. In order to preserve the background profile during action of FR we require u_{TF} and \tilde{u}_{TF} to be equal what leads to the conclusion that the parameter $\tilde{\nu}(t)$, defining change of the aspect ratio of the cigar-shaped trap, must change in time according to the law $\tilde{\nu}(t) = \nu\sqrt{g(t)}$.

Thus, “stable” generation of a train of dark solitons can be achieved by simultaneous application of the FR and of the respective change of the trap potential. The model describing the phenomenon reads

$$i\partial_t\psi = -\partial_x^2\psi + U_0\text{sn}^2(\kappa x, m)\psi + e^{t/\tau}\nu^2x^2\psi + 2e^{t/\tau}|\psi|^2\psi. \quad (72)$$

Examples of initial and final shapes of the condensate density affected by FR and adiabatically varying trap potential within the framework of the model (72) are shown in Figs.10a,b. Fig.10a shows sharpening of the atomic distribution around potential minima. One also observes shifts of the density extrema outwards the minimum of the magnetic trap what occurs due to expansion of the condensate due to the growth of repulsive interactions among atoms.

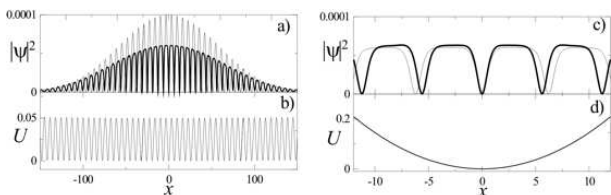


FIG. 10: Initial $t = 0$ (thin line) and final $t = 21$ (thick line) profiles of the condensate (a) and potential (b). Parameters are $\nu = 0.0002$, $\tau = 2$, $\kappa = 0.5$, $m = 0.1$, and $U_0 = 0.05$. (c) dynamics of the dark solitons in the (d) parabolic potential after switching off at $t = 21$ the FR and periodic potential. Thin line corresponds to $t = 21$ and thick for $t = 25$.

In the case at hand free expansion of the condensate is not of interest, because it strongly affects the background. That is why to identify solitons we switch off at some time (in Fig.10 it is $t = 21$) OL, FR and modulation of the parabolic trap, leaving the last one unchanged. As one can see from the Fig.10c, just after that all dark solitons start to move toward the center of the condensate. This happens because of reflection of solitons by the potential boundaries (notice that due to introduced modulation of ν the trap potential has become more narrow than it was at $t = 0$ (see [22])). The difference in the depth of each of solitons causes different velocities and distance which solitons pass by moving to the center, what is also clearly seen in Fig.10.

VI. 3D NUMERICAL SIMULATIONS. THE GENERAL CASE

In the previous sections we considered 1D models of a BEC in an OL, obtained by means of multiple-scale expansion. As it is clear a 1D model cannot take into account all features of the dynamics, what becomes especially relevant in the case of growing nonlinearity. In particular, the later can change significantly the background resulting in failure of the low density approach. That is why now we provide direct numerical study of 3D GP equation (1) for a cigar-shaped condensate having radially symmetric configuration. Using the same dimensionless variables as in Eq.(3) one can rewrite the model in the form

$$i\partial_t\Psi = -\left(\partial_x^2 + \frac{1}{r_\perp}\partial_{r_\perp}r_\perp\partial_{r_\perp}\right)\Psi + (r_\perp^2 + \nu^2x^2)\Psi + U_0\kappa^2\text{sn}^2(\kappa x, m)\Psi + 8\pi\sigma e^{t/\tau}|\Psi|^2\Psi \quad (73)$$

where all tildes are suppressed and it is assumed that the nonlinearity varies according to (69).

By using the assumption about initially weak nonlinearity (see Sec.V) one can consider an initial profile of the condensate as a 1D periodic solution $u_{\text{pq}}(x)$ taken from the Table III [where U_0 must be substituted by κ^2U_0 due to the normalization accepted in Sec. IV (see Eq.(51))]

and modulated by the 3D Gaussian envelope:

$$|\Psi(x, \mathbf{r}_\perp, t = 0)|^2 = u_{\text{pq}}^2(x)e^{-r_\perp^2 - \nu x^2}. \quad (74)$$

A. Dynamics of cn- and dn-waves in a BEC with a negative scattering length

Let us consider dynamics of a BEC described by GP equation (73) with initial density distribution (74) where $u_{\text{pq}}(x)$ taken to be cn-wave, $u_{\text{cn}}(x)$, from Table III. To be more specific, in physical units, the numerical results reported below are obtained for $\mathcal{N} \approx 5 \times 10^3$ atoms of ^7Li loaded in an elongated trap with $\omega_0 = 2\pi \times 1.2$ Hz and $\omega_\perp = 2\pi \times 57.5$ Hz (what gives the aspect ratio $\nu \approx 0.02$). Taking into account that by changing the magnetic field near resonant point 725 G one can change scattering length by order of $\approx 10^2 \div 10^3$ [4], the initial magnitude of the scattering length is chosen to be $a_s(0) = -0.1$ nm. As a matter of fact this corresponds to transfer of the condensate from quasi-linear limit with small nonlinearity to the limit of relatively strong two-body interactions. Indeed, according to the definition of the small parameter (2), in the case at hand its initial values is $\epsilon \approx 0.12$. The respective initial density distribution is shown in Fig.11a and in Figs.12a,b, the later showing the axial ($\mathbf{r}_\perp = 0$) and radial ($x = 0$) cross-sections. The choice of initially weakly-nonlinear condensate allows one to use the results of the 1D theory developed above to predict formation of a train of bright solitons.

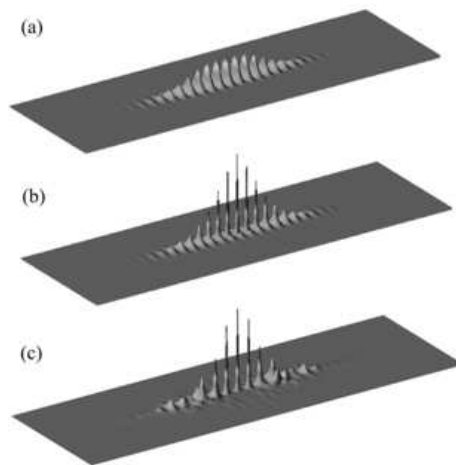


FIG. 11: Dynamics of the condensate density, $|\Psi|^2$, obtained by numerical solution of GP equation (73) with attractive interactions ($\sigma = -1$). Initial density is taken as (74) where parameters of cn-wave are $m = 0.1$, $\kappa = 0.5$ and $\nu = 0.02$. The amplitude of OL is $U_0 = 0.2E_R$. (a) Initial, (b) intermediate ($t_0 = 4.4$ ms) and (c) final ($t_f = 9$ ms) density profiles of the condensate with $\mathcal{N} \approx 5 \times 10^3$ atoms of ^7Li . The characteristic times of FR, i.e. τ in the physical units, is 1 ms. The size of the images in (a)–(c) is $180 \times 40 \mu\text{m}$. The value of the distribution picks is shown in Fig.12.

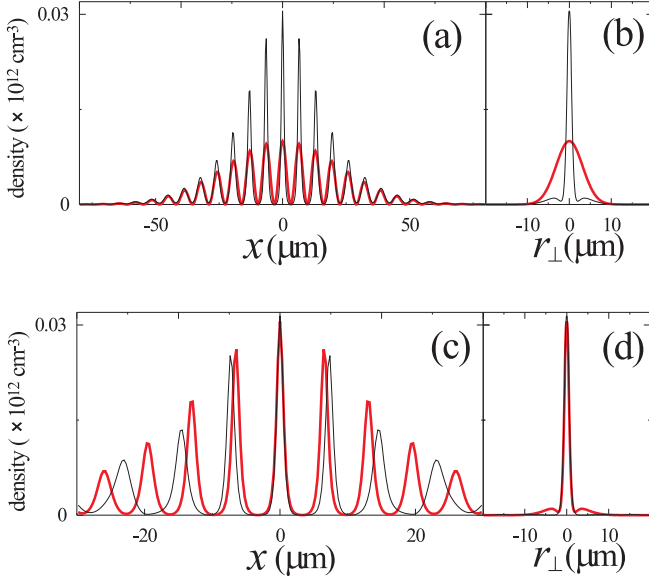


FIG. 12: Cross-sections of the density $|\Psi(\mathbf{r})|^2$, shown in Fig.11 along axial, $\mathbf{r}_\perp = 0$, (a,c) and radial, $x = 0$, (b,d) directions. In (a,b) thick and thin lines correspond to initial $t = 0$ and to intermediate $t = t_0$ times. In (c,d) thick thin lines correspond to intermediate $t = t_0$ and to final $t = t_f$ times.

While FR is switched on (i.e. for $t < 4.4$ ms) the periodic density distribution displays sharpening in each potential well acquiring a shape of quasi-1D soliton train which at $t = 4.4$ ms is shown in Fig.11b and Figs.12a,b. As one can see from Figs.12a,b, appearing of localized excitations is accompanied by appreciable narrowing of the transverse profile of the condensate (evidently not taken into account in the 1D approximation developed above). Axial dimension of the condensate does not change. We also notice that due to choice of relatively weak initial nonlinearity we did not observed collapse.

Next, at the intermediate time $t_0 = 4$ ms (what corresponds to $a_s(t_0) \approx 81.5a_s(0)$ and respectively to increase of ϵ approximately nine times) we switch off FR as well as periodic and trap potentials in the axial direction (leaving only parabolic potential in the radial direction). This allows condensate to expand freely in the axial direction (a kind of a waveguide configuration). A density distribution after 4.6 ms of free 1D expansion is shown in Figs.11c and 12c,d. Now the transverse profile of the condensate changes weakly (see Fig.12d), while localized pulses move outwards the center of the condensate (see Fig.12c). In the 1D approximation such pulses were identified with solitons. This is not so any more when one considers 3D problem. In particular, for low amplitude solitary pulses (they are located on the wings of the condensate) dispersion dominates nonlinearity and one observes spreading out of each pulse. In spite of this spreading, however, they preserve well pronounced spatially localized structure, while moving along the effectively created waveguide in the condensate.

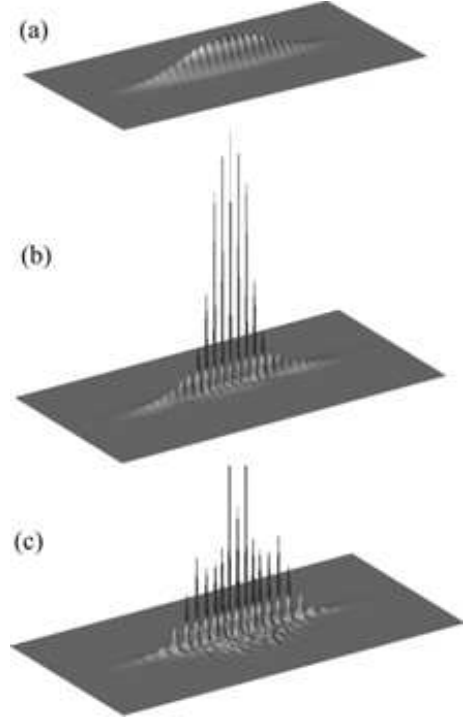


FIG. 13: Dynamics of the condensate density $|\Psi(\mathbf{r})|^2$ obtained by numerical solution of GP equation (73) with attractive interactions ($\sigma = -1$). The initial density distribution (74) is taken as a dn-wave with $m = 0.1$, $\kappa = 1$ and with $\nu = 0.02$. (a) Initial, (b) intermediate ($t_0 = 5.2$ ms) and (c) final ($t_f = 10$ ms) density profiles of the condensate of $\mathcal{N} \approx 10^4$ atoms of ${}^7\text{Li}$. The amplitude of OL is $U_0 = 0.2E_R$. The characteristic time of FR, i. e. τ in physical units, is 2 ms. The size of the images in (a)–(c) is $180 \times 80 \mu\text{m}$.

Next we consider evolution of a dn-wave (where in the initial density distribution (74) $u_{\text{pq}}(x) = u_{\text{dn}}(x)$ from Table III). The initial profile and its cross-sections are shown in Fig.13a and Figs.14a,b, respectively. Now we used the same magnetic trap as in the previous case. Taking $\mathcal{N} \approx 10^4$ of ${}^7\text{Li}$ atoms we obtain the initial value of the small parameter (2) to be ≈ 0.17 . Numerical simulations are carried out in the same way as this was done in the previous example, with the time of FR being $t_0 = 5.2$ ms (what corresponds to $a_s(t_0) \approx 14a_s(0)$) and free 1D expansion of the condensate along the waveguide during 4.8ms between t_0 and $t_f = 10$ ms.

While the FR is switched on one observes strong sharpening of the distribution maxima (much more pronounced than in the case of a cn-wave) with significant narrowing of the transverse profile (see Fig.13b and Figs.14a,b). Meantime, during the free expansion, the condensate displays less regular structure of the train of solitary pulses (see Fig.13c and Fig.14c), what was predicted by the 1D theory on the stability arguments applied to a sequence of the in-phase neighbor pulses. Another peculiarity, found numerically is that oscillatory behavior of the transverse distribution appears, what is

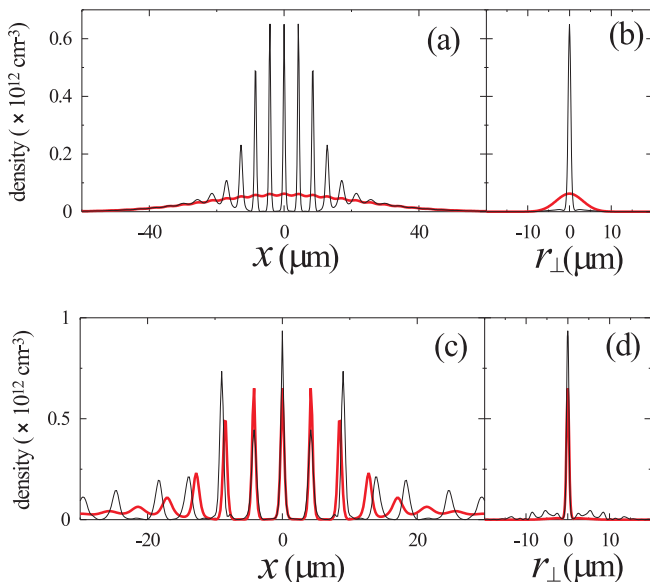


FIG. 14: Cross-sections of the density $|\Psi(\mathbf{r})|^2$ shown in Fig.13 along the axial $r_{\perp} = 0$ (a,c) and radial $x = 0$ (d,e) directions. In (a,b) thick and thin lines correspond to initial $t = 0$ and to intermediate $t = t_0$ times. In (c,d) thick and thin lines correspond to intermediate $t = t_0$ and to final $t = t_f$ times.

clearly seen from Fig.14d.

B. Dynamics of an sn-wave in a BEC with a positive scattering length

As a final example we consider the case of a BEC with repulsive interactions (what corresponds to $\sigma = 1$) where in the initial density distribution (74) the solution u_{pq} is taken in a form of the sn-wave (i.e. as u_{sn} from Table III). In Figs.15 and 16 we present density profiles of the condensate of rubidium atoms, confined by the trap with axial $\omega_0 = 2\pi \times 0.11$ Hz and radial $\omega_{\perp} = 2\pi \times 1.17$ Hz harmonic oscillator frequencies, at different moments of time. It is supposed that initially two body interactions are negligible. The last condition for a given number of atoms can be achieved by proper choice of the external magnetic field: for example, according to [6] in the case of ^{87}Rb atoms the magnetic field can be chosen about 170 G when the magnitude of the scattering length can be made as small as $a_s(0) = 0.1$ nm, what according to (2) gives the small parameter $\epsilon \approx 0.38$, providing the required weakly nonlinear limit. Then by approaching the resonant point (≈ 156 G) one can change magnitude of scattering length by 10^3 times.

As before FR is switched on at $t = 0$ leading to the evolution shown for $t_0 = 30$ ms in Figs.15a,b. One observes decreasing of the amplitude of the density and formation of a sequence of well pronounced excitations having the shape of a train of dark solitons.

As before at some time, precisely at $t_0 = 30$ ms when the scattering length achieves the value $a_s(t_0) =$

$148a_s(0)$, we switch off both FR and OL, but unlike in the previous cases leave the axial parabolic trap. Holding the trap potential is necessary to prevent expansion of the condensate, the later leading to change of the background against which dark solitons are created.

There are two peculiarity of the 3D evolution of the periodic wave to be mentioned here. First, comparing Figs.16c and 10c, one finds that after switching off the FR dark solitons move undergoes shifts in opposite directions (the 3D simulations show solitons moving outwards the center while in 1D simulations solitons move toward the center of the parabolic potential). The second feature of the 3D dynamics is appreciable change of the background. In particular, in Fig.16d one can see significant expansion of the condensate, what results in significant decrease of the amplitude of the background (which can be observed also in Fig.16c). This change of the background caused by the radial expansion of the condensate seems to be responsible for the effect of the “reverse” motion of solitons. Indeed as one can see from Fig.16c decrease of the background amplitude is accompanied by the decrease of soliton amplitude, while more “shallow” solitons are allowed to oscillate in a parabolic potential with larger amplitudes of the deviation from the potential minimum. In other words, in the provided 3D simulations we did not reach the time of reflection of the solitons from the walls of the trap potential.

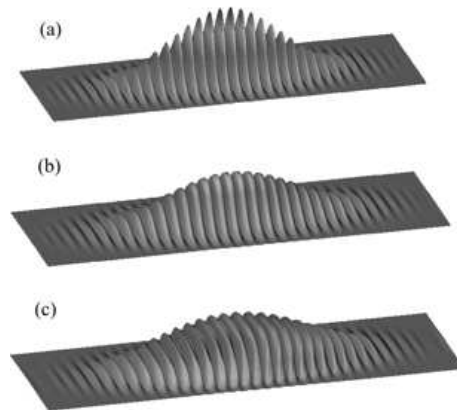


FIG. 15: Dynamics of the condensate density obtained by numerical solution of GP equation (73) with repulsive interactions ($\sigma = 1$). Initial density is taken as an sn-wave with $m = 0.1$ and $\kappa = 0.75$ modulated by the Gaussian function with $\nu = 0.1$. (a) Initial, (b) intermediate ($t_0 = 30$ ms) and (c) final ($t_f = 45$ ms) density profiles of the condensate of $\mathcal{N} \approx 5 \times 10^4$ atoms of ^{87}Rb embedded in 1D OL with the amplitude $U_0 \approx -0.2E_R$. The characteristic time of FR is $\tau \approx 6$ ms. The size of the images in (a)-(c) is $150 \times 60 \mu\text{m}$.

VII. DISCUSSION AND CONCLUSION

In conclusion we investigated formation of trains of matter bright and dark solitons in an elongated BECs

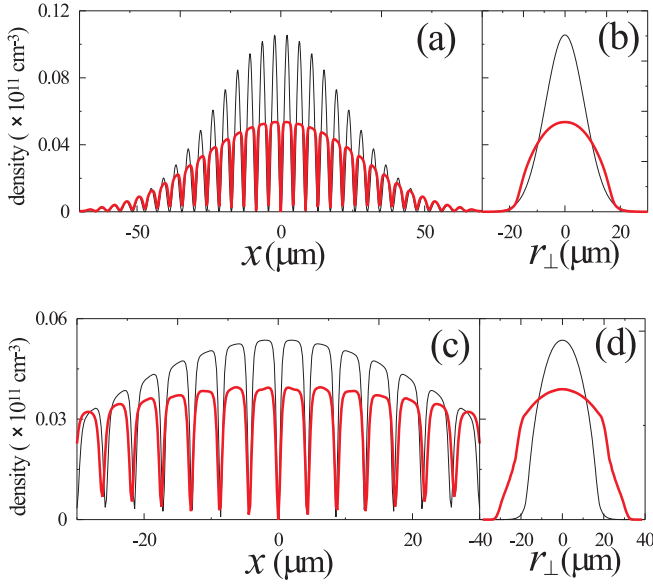


FIG. 16: Cross-sections of the density $|\Psi(\mathbf{r})|^2$ along the axial $\mathbf{r}_\perp = 0$ and radial $x = x_{\max}$ direction (here x_{\max} is a coordinate of the first density peak closest to the center). In (a,b) thin lines correspond to initial $t = 0$ and thick lines to intermediate $t = t_0$ times. In (c,d) thin lines correspond to intermediate $t = t_0$ and thick lines to final $t = t_f$ times. Parameters are the same as in Fig.15.

embedded in OLs by means of adiabatical change of the value of the scattering length. For a cigar-shaped condensate we considered reductions of the initially 3D GP equation to the 1D NLS equation. The resulting 1D equation depends on the relation among main spatial scales of the problem. In particular, parabolic and periodic potentials are included into the final NLS equation either explicitly or through coefficients (see Table I). This was done by using multiple-scale expansion method. Special attention has been paid to discussion of the link between periodic and solitary wave solutions of the 1D NLS equation, what naturally led us to idea how to affect a periodic wave in a BEC loaded in a lattice, in order to create a train of solitons. In a number of cases the phenomenon can be described analytically using adiabatic change of the parameters. When both parabolic and periodic potentials are included explicitly we had to involve numerical simulations in order to obtain wave evolution. The consideration was concentrated on the three types of waves: cn-, dn- and sn-waves. Finally, the process of formation of the trains of bright and dark solitons by means of varying scattering length using FR in the presence of parabolic and periodic potentials was studied in a radially symmetric simulations of real 3D condensates. In the most cases the 1D models provided adequate description of the dynamics. Meantime, it turned out that full 3D consideration may be necessary because of significant deformation of the transverse structure of the condensate. This is in particular the case of trains of dark solitons, which are rather sensitive to the amplitude and structure

of the background, affected by the FR.

The method was shown to be efficient for the sake of creation of solitons, which after being generated can propagate along effective one-dimensional guides for matter solitons, created by parabolic potential in the transverse direction. From the theoretical point of view the method allows controllable creation of solitons, because formally one can indicate *a priori* a value of the scattering length necessary for creation of a given number of solitons.

Acknowledgments

Work of V.A.B. has been supported by the FCT fellowship SFRH/BPD/5632/2001.

APPENDIX A: UV-PAIR

For the sake of convenience here we present the UV-pair for the NLS equation (16) (see e.g. [16])

$$\mathbf{U} = \begin{pmatrix} \frac{\lambda}{\sqrt{\sigma}} & \sqrt{\sigma} \bar{\psi} \\ \sqrt{\sigma} \psi & -\frac{\lambda}{2i} \end{pmatrix} \quad (\text{A1})$$

$$\mathbf{V} = \begin{pmatrix} -\frac{\lambda^2}{2i} + i\tilde{\sigma}|\psi|^2 & -\sqrt{\sigma}(i\bar{\psi}_x + \lambda\bar{\psi}) \\ \sqrt{\sigma}(i\psi_x - \lambda\psi) & \frac{\lambda^2}{2i} - i\tilde{\sigma}|\psi|^2 \end{pmatrix}. \quad (\text{A2})$$

The constant λ is called a spectral parameter. Differentiating equations (20) with respect to t and x correspondingly and requiring them to be satisfied for any value of λ one arrives at the compatibility condition $\mathbf{U}_t - \mathbf{V}_x + [\mathbf{U}, \mathbf{V}] = 0$ and as a consequence, to the NLS equation (16).

APPENDIX B: ON PARAMETRIZATION

Let us rewrite $P(\lambda)$ as $P(\lambda) = \lambda^4 + c_3\lambda^3 + c_2\lambda^2 + c_1\lambda + c_0$. Formulas (23) and (24) suggest that P_{ij} should also be searched in a form of polynomials with respect to the parameter λ (at least of the second order). That is why, we make a substitution

$$\Delta P = \lambda^2 + \lambda\Delta_1 + \Delta_0, \quad P_{12} = \lambda P_{12}^{(1)} + P_{12}^{(0)} \quad (\text{B1})$$

and look for the explicit form of the coefficients Δ_j and $P_{12}^{(j)}$. Comparing powers of λ in (23) we obtain four relations:

$$\Delta_1 = \frac{c_3}{2}, \quad \Delta_0 = 2\tilde{\sigma}|P_{12}^{(1)}|^2 + \frac{1}{2} \left(c_2 - \frac{1}{4}c_3^2 \right), \quad (\text{B2})$$

$$c_3\Delta_0 - 4\tilde{\sigma} \left(\bar{P}_{12}^{(1)} P_{12}^{(0)} + \bar{P}_{12}^{(0)} P_{12}^{(1)} \right) = c_1, \quad (\text{B3})$$

$$\Delta_0^2 - 4\tilde{\sigma}|P_{12}^{(0)}|^2 = c_0. \quad (\text{B4})$$

From the first of Eqs. (22) we compute the equation for $\partial_x P_{12}$ whose consistency with representations (B1) and (B2) results in the following connecting formulas

$$\bar{\psi} = \frac{i}{\sqrt{\sigma}} P_{12}^{(1)}, \quad (\text{B5})$$

$$\bar{\psi}_x = \frac{1}{\sqrt{\sigma}} P_{12}^{(0)} + \frac{i}{2} c_3, \quad (\text{B6})$$

$$\bar{\psi}_{xx} = \bar{\psi} \Delta_0. \quad (\text{B7})$$

Comparing (B7) with (9) one easily verifies that the two equations coincide subject to the conditions $c_2 = 2\omega$ and $c_3 = 0$ what is the same as (25) and (27). It worth pointing out here that in the case of more general solution (19) the sum of the parameters λ_j , i.e. coefficient c_3 , determines the velocity V , and thus (27) expresses the fact that the velocity of the solution we are looking for is equal to zero. Then, it follows from (B5) that $\bar{P}_{12}^{(1)}$ is a solution of (16). If one also takes into account the particular form of the solution (17) one immediately concludes from (B3), (B5), (B6), and (27), that $c_1 = 0$. Finally we compare (B4) with (18) taking into account (17). This gives $C = \frac{\bar{\sigma}}{16}(c_2^2 - 4c_0)$ what is the same as (26).

APPENDIX C: SOME FORMULAS FROM ELLIPTIC INTEGRALS

Throughout the text we use the asymptotic of the elliptic integrals (see e. g. [17, 20]) when $m \rightarrow 1$:

$$\begin{aligned} K(m) &= \ln \frac{4}{\sqrt{1-m}} [1 + O(1-m)], \\ E(m) &= 1 + O[(1-m) \ln(1-m)], \end{aligned} \quad (\text{C1})$$

and when $m \rightarrow 0$

$$\begin{aligned} K(m) &= \frac{\pi}{2} \left[1 + \frac{m}{4} + \left(\frac{3}{8}\right)^2 m^2 + O(m^3) \right], \\ E(m) &= \frac{\pi}{2} \left[1 - \frac{m}{4} - \left(\frac{3}{8}\right)^2 \frac{m^2}{3} + O(m^3) \right]. \end{aligned} \quad (\text{C2})$$

In order to prove that ξ_2 described by (38) is a monotonically decreasing function, we observe that $K(m) \geq E(m)$, and show that

$$2\xi_2 K(m) - (\xi_1 + \xi_2) E(m) \leq 0, \quad (\text{C3})$$

where $m = (\xi_1 - \xi_2)^2 / (\xi_1 + \xi_2)^2$. To this end we introduce the elliptic modulus $k = \sqrt{m}$ and rewrite (C3) as $\mathcal{F}_1(k) \equiv (1-k)K(k^2) - E(k^2) \leq 0$. In order to prove the last formula we use that its left hand side is zero at $k = 0$, and its derivative is given by $d\mathcal{F}_1(k)/dk = -[E(k^2) + K(k^2)]/(1+k) < 0$ (for the last formulas we used [20]: $dE/dk = (E - K)/k$ and $dK/dk = [E(k^2) - k'^2 K(k^2)]/(kk'^2)$ where $k'^2 + k^2 = 1$).

By analogy, in order to show that η_2 in (43) is monotonically increasing function it is enough to verify that $d\mathcal{F}_2(k)/dk = -[K(k^2) - E(k^2)][1 - k']/(kk') < 0$ where $\mathcal{F}_2(k) \equiv k'K(k^2) - E(k^2) \leq 0$.

-
- [1] F. Dalfovo, S. Giorgini, L.P. Pitaevskii, and S. Stringari, Rev. Mod. Phys. **71**, 463 (1999); A.J. Leggett, Rev. Mod. Phys. **73**, 307 (2001); W. Ketterle, Rev. Mod. Phys. **74**, 1131 (2002); E. A. Cornell and C. E. Wieman, Rev. Mod. Phys. **74**, 875 (2002).
- [2] V.A. Brazhnyi and V.V. Konotop, Mod. Phys. Lett. B **18** 627 (2004)
- [3] B.P. Anderson and M.A. Kasevich, Science **282**, 1686 (1998); O. Morsch, J.H. Müller, M. Cristiani, D. Ciampini, and E. Arimondo, Phys. Rev. Lett. **87**, 140402 (2001); M. Cristiani, O. Morsch, J.H. Müller, D. Ciampini, and E. Arimondo, Phys. Rev. A **65**, 063612 (2002); B. Eiermann, P. Treutlein, Th. Anker, M. Albiez, M. Taglieber, K.-P. Marzlin, and M.K. Oberthaler, Phys. Rev. Lett. **91**, 060402 (2003).
- [4] L. Khaykovich, F. Schreck, G. Ferrari, T. Bourdel, J. Cubizolles, L.D. Carr, Y. Castin, and C. Salomon, Science **296**, 1290 (2002); K.E. Strecker, G.B. Partridge, A.G. Truscott, and R.G. Hulet, Nature **417**, 150 (2002).
- [5] W.C. Stwalley, Phys. Rev. Lett. **37**, 1628 (1976); E. Tiesinga, B.J. Verhaar, and H.T.C. Stoof, Phys. Rev. A **47**, 4114 (1993); E. Tiesinga, A.J. Moerdijk, B.J. Verhaar, and H.T.C. Stoof, Phys. Rev. A **46**, R1167 (1992).
- [6] S. Inouye, M.R. Andrews, J. Stenger, H.-J. Miesner, D.M. Stamper-Kurn, and W. Ketterle, Nature **392**, 151 (1998); J. Stenger, S. Inouye, M. R. Andrews, H.-J. Miesner, D.M. Stamper-Kurn, and W. Ketterle, Phys. Rev. Lett. **82**, 2422 (1999); S.L. Cornish, N.R. Claussen, J.L. Roberts, E.A. Cornell, and C.E. Wieman, Phys. Rev. Lett. **85**, 1795 (2000).
- [7] F.Kh. Abdullaev, A.M. Kamchatnov, V.V. Konotop, and V.A. Brazhnyi, Phys. Rev. Lett. **90**, 230402 (2003).
- [8] P.G. Kevrekidis, G. Theocharis, D.J. Frantzeskakis, and B.A. Malomed, Phys. Rev. Lett. **90**, 230401 (2003).
- [9] F.Kh. Abdullaev and M. Salerno, J. Phys. B. **36**, 2851 (2003).
- [10] V.M. Pérez-García, V.V. Konotop, and V.A. Brazhnyi, Phys. Rev. Lett. **92**, 220403 (2004).
- [11] F.Kh. Abdullaev, E.N. Tsoy, B.A. Malomed, and R.A. Kraenkel, Phys. Rev. A **68**, 053606 (2003).
- [12] F.Kh. Abdullaev, B.B. Baizakov, S. A. Darmanyan, V.V. Konotop, and M. Salerno, Phys. Rev. A **64**, 043606 (2001).
- [13] G.L. Alfimov, P.G. Kevrekidis, V.V. Konotop, and M. Salerno, Phys. Rev. E **66**, 046608 (2002).
- [14] V.V. Konotop and M. Salerno, Phys. Rev. A **65**, 021602

- (2002).
- [15] V. V. Konotop, in “*Dissipative solitons*”, ed. by N. Akhmeddiev (Springer, in press).
- [16] L.D. Faddeev and L.A. Takhtajan: *Hamiltonian Methods in the Theory of Solitons* (Springer Verlag, Berlin, 1987).
- [17] M. Abramovitz and I. A. Stegun: *Handbook of Mathematical Functions* (Dover, New York, 1965).
- [18] T. Kawata, J. Phys. Soc. Jpn. **51**, 3381 (1982).
- [19] A.J. Moerdijk, B.J. Verhaar, and A. Axelsson, Phys. Rev. A **51**, 4852 (1995).
- [20] D.K. Lawden: *Elliptic Functions and applications* (Springer-Verlag, New York Inc., 1989).
- [21] J.C. Bronski, L.D. Carr, B. Deconinck, J.N. Kutz, and K. Promislow, Phys. Rev. E **63**, 036612 (2001); J.C. Bronski, L.D. Carr, R. Carretero-Gonzalez, B. Deconinck, J.N. Kutz, and K. Promislow, Phys. Rev. E **64**, 056615 (2001).
- [22] V.A. Brazhnyi and V.V. Konotop, Phys. Rev. A **68**, 043613 (2003).
- [23] G. Boffetta and A.R. Osborne, J. Comput. Phys. **102**, 252 (1992).